

University of Groningen

mTOR-Activating mutations in RRAGD are causative for kidney tubulopathy and cardiomyopathy

Schlingmann, Karl P.; Jouret, François; Shen, Kuang; Nigam, Anukrati; Arjona, Francisco J.; Dafinger, Claudia; Houillier, Pascal; Jones, Deborah P.; Kleinerüschkamp, Felix; Oh, Jun

Published in:
Journal of the American Society of Nephrology

DOI:
[10.1681/ASN.2021030333](https://doi.org/10.1681/ASN.2021030333)

IMPORTANT NOTE: You are advised to consult the publisher's version (publisher's PDF) if you wish to cite from it. Please check the document version below.

Document Version
Publisher's PDF, also known as Version of record

Publication date:
2021

[Link to publication in University of Groningen/UMCG research database](#)

Citation for published version (APA):

Schlingmann, K. P., Jouret, F., Shen, K., Nigam, A., Arjona, F. J., Dafinger, C., Houillier, P., Jones, D. P., Kleinerüschkamp, F., Oh, J., Godefroid, N., Eltan, M., Güran, T., Burtsey, S., Parotte, M. C., König, J., Braun, A., Bos, C., Serra, M. I., ... de Baaij, J. H. F. (2021). mTOR-Activating mutations in RRAGD are causative for kidney tubulopathy and cardiomyopathy. *Journal of the American Society of Nephrology*, 32(11), 2885–2899. <https://doi.org/10.1681/ASN.2021030333>

Copyright

Other than for strictly personal use, it is not permitted to download or to forward/distribute the text or part of it without the consent of the author(s) and/or copyright holder(s), unless the work is under an open content license (like Creative Commons).








The publication may also be distributed here under the terms of Article 25fa of the Dutch Copyright Act, indicated by the "Taverne" license. More information can be found on the University of Groningen website: <https://www.rug.nl/library/open-access/self-archiving-pure/taverne-amendment>.

Take-down policy

If you believe that this document breaches copyright please contact us providing details, and we will remove access to the work immediately and investigate your claim.

Downloaded from the University of Groningen/UMCG research database (Pure): <http://www.rug.nl/research/portal>. For technical reasons the number of authors shown on this cover page is limited to 10 maximum.

mTOR-Activating Mutations in *RRAGD* Are Causative for Kidney Tubulopathy and Cardiomyopathy

Karl P. Schlingmann ¹, François Jouret ^{2,3}, Kuang Shen,^{4,5,6,7,8} Anukrati Nigam,⁹ Francisco J. Arjona,¹⁰ Claudia Dafinger,^{11,12} Pascal Houillier,^{13,14,15} Deborah P. Jones,¹⁶ Felix Kleinerüschkamp,¹⁷ Jun Oh,¹⁸ Nathalie Godefroid,¹⁹ Mehmet Eltan,²⁰ Tülay Güran,²⁰ Stéphane Burtey,²¹ Marie-Christine Parotte,²² Jens König,¹ Alina Braun,^{11,12} Caro Bos ¹⁰, Maria Ibars Serra,¹⁰ Holger Rehmann,²³ Fried J.T. Zwartkuis ²³, Kirsten Y. Renkema ⁹, Karin Klingel,²⁴ Eric Schulze-Bahr ²⁵, Bernhard Schermer,^{12,26} Carsten Bergmann,^{27,28} Janine Altmüller,²⁹ Holger Thiele,²⁹ Bodo B. Beck ^{30,31,36}, Karin Dahan,^{32,33} David Sabatini,^{4,5,6,7} Max C. Liebau ^{11,12,36}, Rosa Vargas-Poussou ³⁴, Nine V.A.M. Knoers ³⁵, Martin Konrad,¹ and Jeroen H.F. de Baaij ¹⁰

Due to the number of contributing authors, the affiliations are listed at the end of this article.

ABSTRACT

Background Over the last decade, advances in genetic techniques have resulted in the identification of rare hereditary disorders of renal magnesium and salt handling. Nevertheless, approximately 20% of all patients with tubulopathy lack a genetic diagnosis.

Methods We performed whole-exome and -genome sequencing of a patient cohort with a novel, inherited, salt-losing tubulopathy; hypomagnesemia; and dilated cardiomyopathy. We also conducted subsequent *in vitro* functional analyses of identified variants of *RRAGD*, a gene that encodes a small Rag guanine triphosphatase (GTPase).

Results In eight children from unrelated families with a tubulopathy characterized by hypomagnesemia, hypokalemia, salt wasting, and nephrocalcinosis, we identified heterozygous missense variants in *RRAGD* that mostly occurred *de novo*. Six of these patients also had dilated cardiomyopathy and three underwent heart transplantation. We identified a heterozygous variant in *RRAGD* that segregated with the phenotype in eight members of a large family with similar kidney manifestations. The GTPase RagD, encoded by *RRAGD*, plays a role in mediating amino acid signaling to the mechanistic target of rapamycin complex 1 (mTORC1). RagD expression along the mammalian nephron included the thick ascending limb and the distal convoluted tubule. The identified *RRAGD* variants were shown to induce a constitutive activation of mTOR signaling *in vitro*.

Conclusions Our findings establish a novel disease, which we call autosomal dominant kidney hypomagnesemia (ADKH-*RRAGD*), that combines an electrolyte-losing tubulopathy and dilated cardiomyopathy. The condition is caused by variants in the *RRAGD* gene, which encodes Rag GTPase D; these variants lead to an activation of mTOR signaling, suggesting a critical role of Rag GTPase D for renal electrolyte handling and cardiac function.

JASN 32: 2885–2899, 2021. doi: <https://doi.org/10.1681/ASN.2021030333>

The kidney tubule balances fluid, electrolyte, and mineral homeostasis. The genetic deciphering of hereditary disturbances of electrolyte reabsorption by the tubule, collectively known as tubulopathies, has greatly improved the understanding

of electrolyte transport along the nephron.^{1,2} Over the last decade, we and others have identified critical components of epithelial magnesium ion (Mg^{2+}) reabsorption pathways in the thick ascending limb of the loop of Henle (TAL) and the distal

convoluted tubule (DCT).^{2,3} In the TAL, 50%–70% of the filtered Mg^{2+} is reabsorbed paracellularly *via* the claudin16–19 complex.⁴ This paracellular Mg^{2+} transport is dependent on the transcellular salt reabsorption and negatively regulated by the basolateral calcium-sensing receptor.^{3,5} In the DCT, Mg^{2+} reabsorption is mediated by transient receptor potential melastatin type 6 and 7 (TRPM6/TRPM7) channels.^{6–12}

In our cohort of patients with hypomagnesemia, we noted a subset of patients sharing a tubulopathy characterized by (1) renal salt wasting, (2) profound hypomagnesemia, and (3) nephrocalcinosis, combined with a dilated cardiomyopathy (DCM). Because DCM had not been described in patients with known hereditary forms of hypomagnesemia,² we hypothesized that these individuals were affected by a yet-undefined disease phenotype. By next-generation sequencing, we identified *Ras-related GTP binding D (RRAGD)* variants in eight unrelated individuals, and in eight members of a large family with symptomatic hypomagnesemia.

METHODS

Subjects

We initially studied a cohort of six individuals with a phenotype combining DCM and a complex renal tubular disorder, including hypomagnesemia (median serum magnesium level of 0.42 mmol/L). Our second cohort consisted of three additional families in which the index patients presented with an isolated tubulopathy. Clinical and biologic data at the time of disease manifestation were collected retrospectively from medical charts. We re-evaluated all patients and obtained follow-up biochemical data. The detailed clinical history of each individual is provided in the Supplemental Appendix 2. All genetic studies were approved by the local ethics committees in Paris, Münster, and Liège, and informed consent was obtained from all subjects and/or their parents.

Serum magnesium, potassium, and chloride levels of individuals with *RRAGD* mutations were statistically compared with nonaffected family members. Samples were tested for normal distribution using the Kolmogorov–Smirnov test. For statistical analyses, a one-sided *t* test in case of normal

Significance Statement

Although advances in genetic techniques have resulted in the identification of rare hereditary disorders of renal magnesium and salt handling, some patients with tubulopathy lack a genetic diagnosis. In a cohort of patients with profound hypomagnesemia, renal salt wasting, nephrocalcinosis, and dilated cardiomyopathy, the authors performed whole-exome and -genome sequencing and identified heterozygous variants in *RRAGD*, which encodes a small Rag guanosine triphosphatase (GTPase). Subsequent functional analyses *in vitro* showed that the identified variants induce a constitutive activation of mechanistic target of rapamycin (mTOR) signaling *in vitro*. These findings not only establish a novel monogenic disorder of the kidney tubule, but demonstrate the essential role of mTOR signaling for distal tubular electrolyte handling and cardiac function.

distribution and a one-sided Mann–Whitney *U* test in case of non-normal distribution were used.

Sequencing

Patients F1.1–F4.1 were subjected to whole-exome sequencing (WES; for details see Supplemental Appendix 1). Exome data were analyzed for shared genes with variants under all modes of inheritance. After discovery of heterozygous *RRAGD* variants in these four patients, two additional patients with DCM and renal tubulopathy were analyzed by conventional Sanger sequencing (F5.1 and F6.1). The analyses were then expanded to 25 patients with a similar renal tubular disorder, but without a known cardiac phenotype, which revealed two additional patients (F7.1 and F8.1).¹³

Due to the lack of genetic material, a *RRAGD* mutation could not be confirmed in the affected father of individual F4.1 who died from DCM at 41 years of age. Of note, an older sister of individual F7.1 died in infancy from acute cardiac failure during a pneumonia episode and the autopsy revealed DCM. Careful genetic re-evaluation revealed mosaicism (17%) in leukocytes of the healthy mother for the respective *RRAGD* mutation (see Supplemental Appendix 2).

We analyzed family F9, which had multiple members affected by isolated renal tubular disease, independently under the assumption of an autosomal dominant disease by whole-genome sequencing (WGS). For this purpose, DNA samples of members III.1, III.6, and IV.2 of family 9 were subjected to WGS on the Illumina X Ten platform (Hartwig Medical Foundation, Amsterdam, The Netherlands). Data analysis was performed by mapping paired end reads (2×100 bp) from the NextSeq instrument against the hg19 human reference genome using the Burrows–Wheeler Aligner with recommended standard settings. Filtering steps excluded common single nucleotide polymorphisms (>1%), introns, untranslated regions, synonymous variants, and low-coverage regions (less than five reads). Overlaps of the remaining variants were generated using VCFMiner to

Received March 12, 2021. Accepted July 7, 2021

K.P.S., F.J., K.S., M.K., and J.H.F.d.B. contributed equally to this work.

Published online ahead of print. Publication date available at www.jasn.org.

Correspondence: Dr. Karl P. Schlingmann, Department of General Pediatrics, University Children's Hospital Münster, Albert Schweitzer Campus 1, 48149 Münster, Germany, or Dr. Jeroen H.F. de Baaij, Department of Physiology, Radboud Institute for Molecular Life Sciences, Radboudumc, P.O. Box 9101, 6500HB, Nijmegen, The Netherlands. Email: karlpeter.schlingmann@ukmuenster.de or jeroen.debaaij@radboudumc.nl

Copyright © 2021 by the American Society of Nephrology

select genes that were present in F1.1–F4.1, which resulted in the identification of one remaining gene, *RRAGD*.¹⁴ An extensive description of the sequencing procedure has been provided in the Supplemental Appendix 1.

Later, two additional patient cohorts were examined: (1) a cohort with isolated tubulopathy and suspected diagnosis of Gitelman syndrome ($n=58$) who had been subjected to WES; and (2) a cohort of patients with dilated cardiomyopathy ($n=74$), in whom mutations in known cardiomyopathy genes had previously been excluded by targeted exome sequencing of 174 cardiovascular genes, including 49 cardiomyopathy genes, as previously described.¹⁷

Cell Lysates and Immunoprecipitation

Human embryonic kidney (HEK293T) cells were transfected with Flag-S6K1, RagA, and RagD mutants, as described previously.¹⁵ To determine the response of mechanistic target of rapamycin complex 1 (mTORC1) to amino acid stimulation or starvation under the control of Rag mutants, 2 million HEK293T cells were plated onto a 10-cm dish. Twenty-four hours later, the cells were transfected with 2 ng of S6K1 and 100 ng of each Rag wild-type (wt) or mutant construct. Thirty-six hours later, amino acid stimulation or starvation was performed for 0.5–1 hour. Cells were rinsed once with ice-cold PBS and lysed with Triton X-100 lysis buffer (40 mM sodium-HEPES, pH 7.4; 5 mM magnesium chloride; 100 mM ATP; 10 mM tetrasodium pyrophosphate; 10 mM sodium β -glycerol phosphate; 1% vol/vol Triton X-100; and one tablet of protease inhibitor cocktail per 25 ml of buffer). The lysates were cleared by centrifugation at 15,000 rpm at 4°C in a microcentrifuge for 10 minutes. For immunoprecipitations, the FLAG M2 beads were pre-equilibrated in Triton X-100 lysis buffer. Thirty microliters of a 50/50 slurry of the FLAG M2 affinity beads were then added to cleared lysates and incubated at 4°C for 2 hours. After immunoprecipitation, the beads were washed one time with Triton X-100 lysis buffer and three times with Triton X-100 lysis buffer supplemented with 500 mM sodium chloride. Immunoprecipitated proteins were denatured by the addition of 50 μ l of 2.5 \times SDS buffer, resolved by SDS-PAGE, and analyzed by immunoblotting.

Sample Preparation for Interactome Analysis

FlpIn inner medullary collecting duct cells stably expressing green fluorescent protein (GFP)–GFP, GFP-Rragd-wt, or GFP-Rragd-Ser75Leu fusion proteins were generated as described previously.¹⁶ Lysates were cleared by centrifugation, followed by incubation with GFP μ MACS magnetic beads (Miltenyi) for 1 hour. Then, lysates were loaded on a μ MACS column and precipitated proteins were GSH, alkylated, and on-column digestion was performed overnight, as previously described.¹⁶ Eluates were acidified the next day using 1%–2% formic acid and stage-tip cleanup was

performed, as previously described, and samples were dried using a vacuum centrifuge. Peptides were resuspended in 0.1% formic acid and were separated using a 1-hour gradient on an nLC coupled to a Q Exactive Plus tandem mass spectrometer (Thermo Scientific) or an LTQ orbitrap XL mass spectrometer. Experimental details are provided in the Supplemental Appendix 1.

Expression Analysis

Total RNA was extracted from the tissues of C57BL/6 mice and isolated DCT cells of parvalbumin-GFP mice using TRIzol Reagent (Thermo Fisher Scientific, Waltham, MA) according to the manufacturer's protocol. To remove genomic DNA, the isolated RNA was subsequently subjected to DNase (Promega, Madison, WI) treatment. RNA was reverse transcribed using Moloney murine leukemia virus reverse transcription (Thermo Fisher Scientific) for 1 hour at 37°C. *Rragd* (forward, CACCTGAGCTTTTACCTGA; reverse, TCAGCAGATTCTCCAGCGTC) gene expression levels were quantified by SYBR Green (Bio-Rad) on a CFX96 Real-Time PCR Detection System (Bio-Rad) and normalized for glyceraldehyde 3-phosphate dehydrogenase (forward, TAACATCAAATGGGGTGAGG; reverse, GGTTACACCCATCACAAC) expression levels.

Immunohistochemistry was performed on kidney tissues of C57BL/6 mice using primary antibodies against RagD, aquaporin-2 (AQP2), sodium chloride cotransporter (NCC), and uromodulin (UMOD), as described previously.¹⁷ Paraffin-embedded kidney sections were subjected to deparaffinization and rehydration, followed by permeabilization in 0.3% (vol/vol) PBS–Triton X-100 (Sigma). Sections were incubated overnight at 4°C with the primary antibodies sheep anti-NCC (1:400, sheep S965B; Medical Research Council Protein Phosphorylation and Ubiquitylation Unit, Dundee, United Kingdom), sheep anti-Tamm Horsfall (1:200, MBS220487; Bio-Trend), and guinea pig anti-AQP2 (1:100; kindly provided by Dr. Peter Deen) and subsequently incubated overnight at 4°C with the primary antibody rabbit anti-RRAGD (1:2000, NBP2-32106; Novus Biologicals). Experimental details are provided in the Supplemental Appendix 1.

RESULTS

Patients

We initially identified eight unrelated individuals with hypomagnesemia and a complex renal tubulopathy phenotype (Table 1), accompanied by muscle spasms and seizures in three individuals. Inappropriately high fractional excretion rates of magnesium indicated renal magnesium wasting (Table 1). In individual F2.1, a magnesium loading test was performed, which disclosed a decreased renal tubular

Table 1. Clinical and laboratory characteristics of patients with RRAGD mutations

Individuals	F1.1	F2.1	F3.1	F4.1	F5.1	F6.1	F7.1	F8.1	F9.1	Family 9 Median (n=8)
Origin	US	France	France	Belgium	Germany	Belgium	Germany	Turkey	Belgium	Belgium
Sex	M	F	F	M	F	M	F	M	M	4F/4M
Age at manifestation	3 yr	3 yr	6 mo	5 yr	7 mo	14 yr	2 yr	6 yr	20 yr	2.5–24 yr
Initial findings	Yes (3 yr)	Yes (12 yr)	Yes (6 mo)	No	Yes (7 mo)	Yes (14 yr)	Yes (4 yr)	No	No	No
Dilated cardiomyopathy (age at diagnosis)	7	8	15	31	15	—	18	—	—	—
Fractional shortening (%; N>25)	15	31	—	61	16	50	—	—	—	—
Ejection fraction (%; N=55–70)	53	55	33	34	42	—	46	—	—	—
Left ventricular end-diastolic diameter (mm) ^a	>P99.9 ^d	>P99.9 ^d	P99.7 ^d	P17.1 ^d	>P99.9 ^d	—	>P99.9 ^d	—	—	—
Hypomagnesemia-related symptoms	No	Tetany	Cerebral seizure	Tetany, muscle cramps	No	No	No	Cerebral seizure	Tetany, muscle cramps	7/8
Nephrocalcinosis	Yes	Yes	Yes	No	Yes	No	Yes	Yes	No	1/8
Polyuria ^b	No	No	Yes	No	Yes	No	Yes	Yes	Yes	2/8
Metabolic alkalosis	No	?	Yes	Yes	No	No	No	Yes	Yes	4/8
Initial laboratory findings	135	—	137	137	141	136	142	141	140	139
S-Na (mmol/L; N=138–145)	4.7	3.2	3.5	3.4	3.5	3.5	3.9	2.7	3.5	3.3
S-K (mmol/L; N=3.5–5.0)	98	—	95	—	100	95	105	91	95	98.5
S-Cl (mmol/L; N=98–106)	2.05	1.78	2.20	2.2	2.11	2.37	2.50	1.8	2.41	2.36
S-Ca (mmol/L; N=2.20–2.70)	0.50	0.27	0.40	0.43	0.40	0.42	0.54	0.26	0.54	0.49
S-Mg (mmol/L; N=0.60–0.95)	1.56	—	1.44	1.59	1.50	—	1.53	1.7	0.87	1.00
S-PO ₄ (mmol/L; N=1.20–1.80)	0.51	0.70	0.24	0.23	0.21	0.75	0.30	0.47	0.74	0.51
S-creatinine (mg/dl)	—	—	24	29.3	—	—	28.5	29.1	—	—
S-HCO ₃ (mmol/L; N=22–29)	33	—	17	29	37	—	91	108	21	18
iPTH (pg/ml; N=9–65)	1.0	—	0.34	0.4	0.8	—	0.9	0.34	0.4	0.40
FE-Na (%; N<2)	13	—	27	6.3	24	—	23	14	7.5	6.2
FE-K (%; N=4–16)	0.67	1.8	1.24 ^c	0.12	1.46 ^c	—	2.27	1.38	0.25	—
Ca-Crea ratio (mol/mol; N<0.9)	47	13.2	7.0	4.3	16	—	13.2	13.8	3.7	—
FE-Mg (%; N<4)	6	—	20	14	10	35	5	19	40	2.5–61
Follow-up findings	Yes (3.3 yr)	Yes (25 yr)	Yes (15 yr)	No	No	No	No	No	No	No
Age at last follow-up (yr)	d.n.a.	d.n.a.	d.n.a.	33	22	14	28	38	—	—
Heart transplant (age)	d.n.a.	d.n.a.	d.n.a.	62	41	45	50	67	78	60–78
Fractional shortening (%; N>25)	d.n.a.	d.n.a.	d.n.a.	37	42	49	43	48	—	—
Ejection fraction (%; N=55–70)	d.n.a.	d.n.a.	d.n.a.	P1.8 ^d	P77.3 ^d	—	>P99.9 ^d	—	—	—
Left ventricular end-diastolic diameter (mm) ^a	d.n.a.	d.n.a.	d.n.a.	—	—	—	—	—	—	—

Table 1. Continued

Individuals	F1.1	F2.1	F3.1	F4.1	F5.1	F6.1	F7.1	F8.1	F9.1	Family 9 Median (n=8)
Most recent laboratory findings										
S-Na (mmol/L; N=135–145)	138	—	140	140	139	140	142	141	140	140
S-K (mmol/L; N=3.5–5.0)	4.6	—	3.7	3.3	3.3	4.6	3.2	3.5	3.5	3.4
S-Cl (mmol/L; N=98–107)	104	—	100	100	100	103	104	95	97	98
S-Ca (mmol/L; N=2.20–2.65)	2.57	—	2.34	2.41	2.50	2.42	2.40	2.27	2.3	2.4
S-Mg (mmol/L; N=0.7–1.1)	0.58	—	0.43	0.55	0.50	0.62	0.66	0.53	0.46	0.48
S-creatinine (mg/dl)	0.47	—	0.64	0.52	0.60	1.18	0.40	0.69	0.67	0.57
S-HCO ₃ (mmol/L; N=22–26)	23.0	—	28.0	25.0	27.0	24.1	24.2	29.9	35.0	29.4
iPTH (pg/ml; N=10–65)	94	—	54	/	34	17.4	60	41	18	17
FE-Na (%; N<2)	1.0	—	1.00	0.34	1.04	0.67	0.9	0.79	0.77	0.57
FE-K (%; N=4–16)	15.5	—	11.0	33.7	18.9	13.8	34	18.2	12.1	10.7
FE-Cl (%)	2.71	—	—	—	1.52	—	—	—	—	—
Ca-Crea ratio (mol/mol; N<0.9)	0.34	—	0.09	0.22	0.25	1.02	1.14	0.08	0.37	—
FE-Mg (%; N<4)	26.0	—	6.3	17.5	12.8	3.3	9.4	14.6	5.9	5.2
Therapy										
Magnesium supplementation	Yes	?	Yes	Yes	Yes	Yes	Yes	Yes	Yes	6/8
Potassium supplementation	No	?	Yes	Yes	Yes	No	Yes	Yes	No	3/8
Heart failure medication	Yes	?	Yes	No	Yes	Yes	Yes	No	No	0/8
Genetic findings (RRAGD mutations)										
Nucleotide level	c.227C>T	c.356C>G	c.662T>A	c.227C>T	c.356C>G	c.227C>T	c.356C>T	c.227C>G	c.289A>C	c.289A>C
Protein level	p.Ser76Leu	p.Pro119Arg	p.Ile221Lys	p.Ser76Leu	p.Pro119Arg	p.Ser76Leu	p.Pro119Leu	p.Ser76Trp	p.Thr97Pro	p.Thr97Pro
Inheritance	De novo	De novo	De novo	Dominant?	De novo	De novo	Maternal mosaicism	De novo	Dominant	Dominant

US, United States; M, male; F, female; ?, unknown; S, serum; Na, sodium; K, potassium; Cl, chloride; Mg, magnesium; PO₄, phosphate; HCO₃, bicarbonate; iPTH, intact parathyroid hormone; FE, fractional excretion; Ca-crea ratio, calcium-creatinine ratio; d.n.a., does not apply.

^aCalculations according to Pettersen et al.³⁷

^b>2 L/m² body surface area per day.

^cMolar Ca-crea ratio N <2.2 for infants.

^dP = percentile of reference weight and height adjusted reference values.

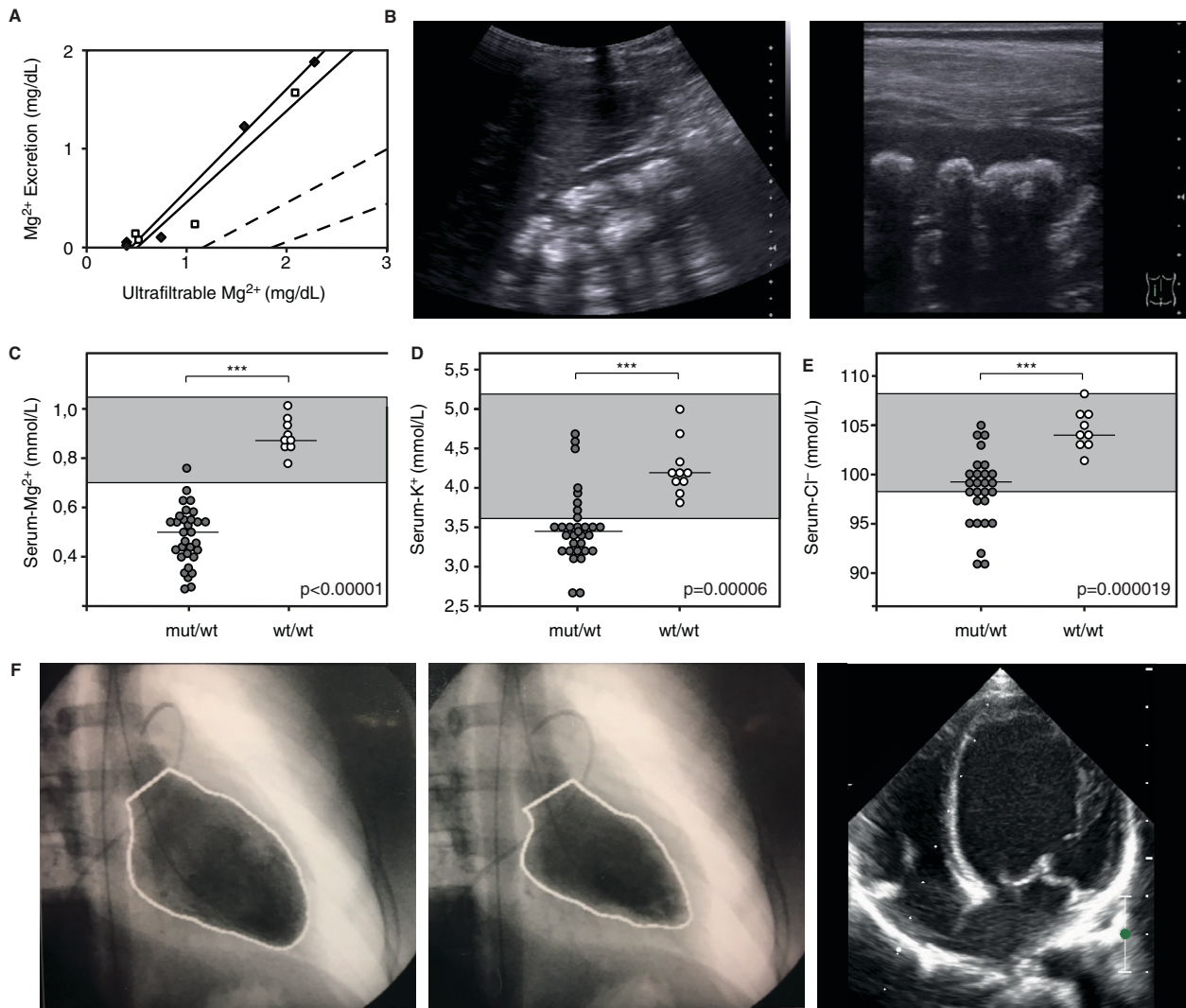


Figure 1. Patients have dilated cardiomyopathy and renal tubulopathy. (A) Magnesium loading test in individual F2.1. Urinary magnesium excretion is plotted against the ultrafiltrable fraction of serum magnesium before and during parenteral infusion of magnesium at increasing concentrations (two separate tests, indicated by open and closed boxes). The dashed lines represent the normal range. (B) Renal ultrasound of individual F7.1 showing severe medullary nephrocalcinosis (grade III according to Hoyer).⁵⁶ (C–E) Comparison of serum magnesium, potassium, and chloride levels of individuals with *RRAGD* mutations (shaded circles) and of unaffected family members (open circles) (initial as well as follow-up values included). Horizontal bars represent medians; reference ranges for serum electrolytes are indicated by gray boxes. Apart from significant hypomagnesemia, individuals with *RRAGD* mutations exhibited significantly lower serum potassium and serum chloride levels, reflecting renal salt wasting. *** $P < 0.001$, one-sided *t* test (magnesium, chloride) and Mann–Whitney *U* test (potassium). (F) Left ventriculography (performed at the age of 12 years) of individual F2.1 who presented with cardiomyopathy. Pictures show left ventricular volumes during diastole (left) and systole (middle), demonstrating a reduced ejection fraction of 40% (normal, 55%–70%). Initial echocardiogram (right) of individual F7.1 performed after genetic diagnosis (apical four-chamber view) showing the dilated left ventricle. Cl⁻, chloride ion; K⁺, potassium ion; mut, mutant.

threshold for magnesium reabsorption (Figure 1A). Additional renal findings included polyuria, hypokalemia, hypochloremia, a tendency toward metabolic alkalosis, hypercalciuria, and nephrocalcinosis, pointing to a defect in the TAL (Figure 1, B–E, Table 1). Of note, the prenatal course of individuals F3.1 and F4.1 was complicated by

polyhydramnios, as observed in antenatal Bartter syndrome.¹⁸ All family members of these probands were clinically unaffected. In six patients (F1–F6), the tubulopathy was accompanied by early and severe DCM. Indeed, three patients (F1.1, F3.1, and F5.1) initially presented in infancy with clinical signs of cardiac insufficiency,

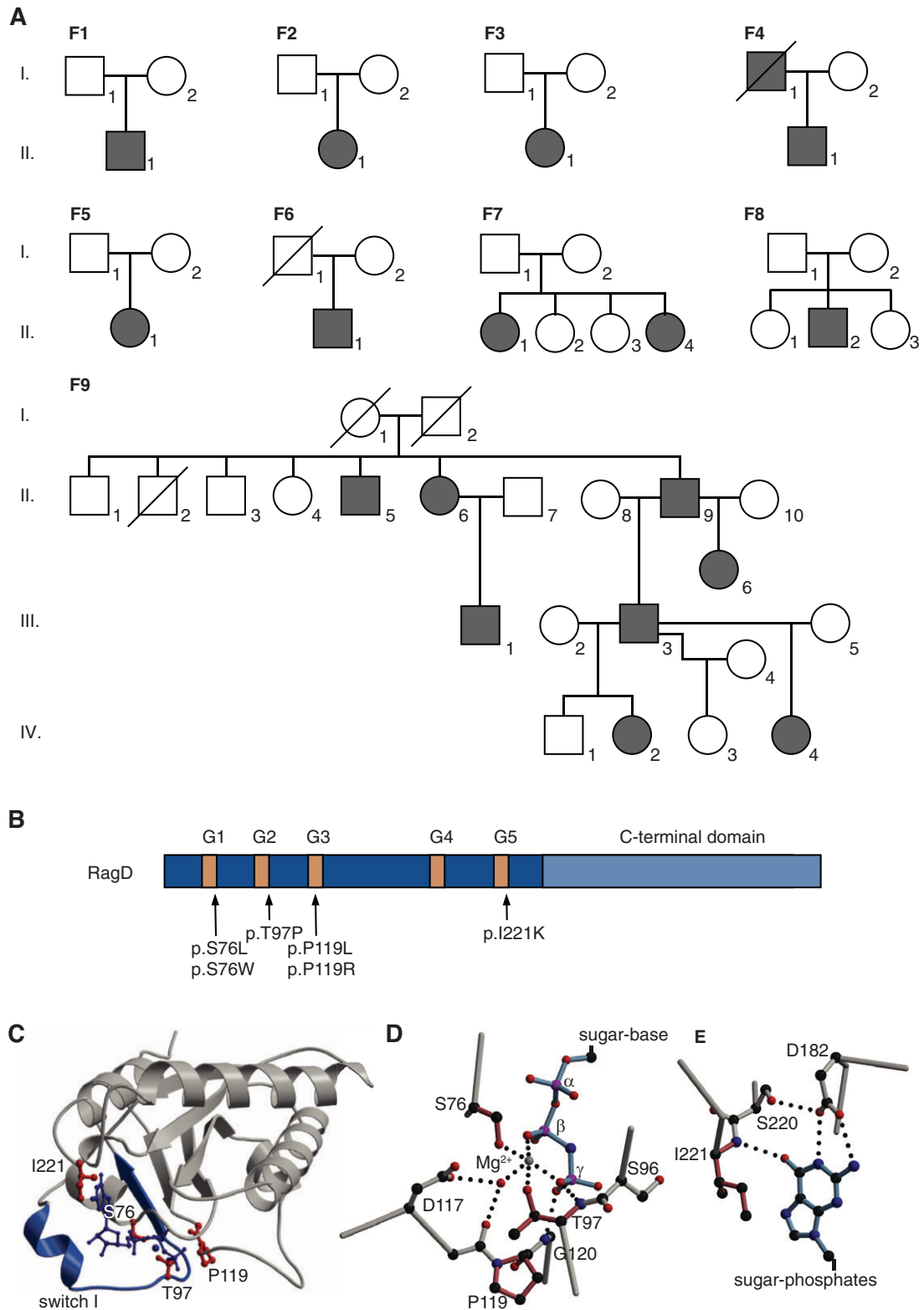


Figure 2. Mutations in the RagD protein are located in the GTP-binding sites. (A) Pedigrees of all families included in this study. Filled symbols represent affected individuals. Squares indicate male family members and circles represent female family members. (B) Domain organization of RagD with GTP-binding motifs in dark blue (G1–G5). Mutations are indicated with an arrow. (C) Crystal structure of RagD in complex with a GTP analogue (GppNHp; Protein Data Bank entry 2q3f). Mutated residues are shown in red. GppNHp and the coordinated Mg^{2+} are depicted in dark blue. (D and E) Detailed view of the (D) phosphate moiety of the nucleotide and (E) the nucleotide base. Affected residues are colored in light red. Dotted lines indicate hydrogen bonds.

including feeding difficulties, vomiting, failure to thrive, sweating, tachycardia, and tachypnea (detailed clinical descriptions are provided in the Supplemental Appendix 2). DCM resulted in heart failure in individuals F1.1–F3.1. Therefore, they received a heart transplantation (Figure 1F). Whereas echocardiography demonstrated a preserved cardiac function at adolescent age in patient F4.1, patients F5.1–F7.1 had an impaired but stable left ventricular function under heart failure medication. Of the patients with DCM, solely patient F3.1 received a loop diuretic before the diagnosis of her tubulopathy, making a contribution of diuretic treatment to the development of medullary nephrocalcinosis, which was observed in the majority of patients, unlikely.

Two patients (F7.1 and F8.1) clinically presented in infancy and early childhood with severe hypomagnesemia and signs of renal salt wasting. Patient F8.1 still displays an unremarkable cardiac function at adult age. In contrast, the initial cardiac evaluation of patient F7.1 after genetic diagnosis revealed DCM and a significantly impaired cardiac function requiring heart failure treatment.

In parallel to these eight unrelated patients, we analyzed a large family (F9; Figure 2A) with eight affected members presenting with profound and symptomatic hypomagnesemia resistant to oral magnesium supplements (pedigree and clinical details in Figure 2 and Supplemental Table 1, respectively). The index patient presented in early adulthood with muscle cramps and tetany. Affected individuals of family F9 exhibited hypokalemia, metabolic alkalosis, and an activation of the renin-angiotensin-aldosterone system (RAAS) together with normal or low BP, suggesting the diagnosis of Gitelman syndrome (Figure 1C, Table 1). None of these individuals showed cardiac abnormalities.

To characterize the renal salt wasting phenotype in more detail, serum potassium and chloride levels were compared between affected individuals ($n=16$) and available nonaffected family members ($n=8$) (Figure 1, D and E). These analyses demonstrated significantly lower values in affected individuals that, together with metabolic alkalosis and RAAS activation, was highly indicative of renal salt wasting.

Identification of RRAGD Mutations

After exclusion of mutations in known genes for hypomagnesemia and salt wasting, we performed WES in individuals F1.1–F4.1, which revealed *RRAGD* as a single common mutated gene (Figure 2B). Subsequently, additional heterozygous *RRAGD* mutations were discovered in patients F5.1 and F6.1, and in patients F7.1 and F8.1 with isolated tubulopathy. Sequencing of unaffected parents demonstrated that the identified *RRAGD* mutations mostly occurred *de novo*. Due to the lack of genetic material, a *RRAGD*

mutation could not be confirmed in the affected father of patient F4.1, who died from DCM at 41 years of age. Of note, an older sister of patient F7.1 died in infancy from acute cardiac failure during a pneumonia episode and the autopsy revealed DCM. Careful genetic re-evaluation revealed mosaicism (17%) in leukocytes of the healthy mother for the respective *RRAGD* mutation (see Supplemental Appendix 2). Family F9, with multiple affected family members, was initially analyzed separately under the assumption of a dominant trait. After exclusion of known genes for hypomagnesemia, WGS revealed a heterozygous *RRAGD* mutation (p.Thr97Pro) that segregated with the disease. Retrospectively, two-point linkage was performed resulting in a suggestive LOD score of 2.41 as evidence for linkage between the mutation and the disease phenotype. The reanalysis and screening of two additional cohorts with either suspected Gitelman syndrome ($n=58$) or isolated DCM did not identify additional pathogenic *RRAGD* variants.

RRAGD encodes a small Rag guanosine triphosphatase (GTPase), which is a member of the Ras family of GTP-binding proteins.¹⁹ All RagD mutations affect highly conserved amino acid residues in GTP-binding domains conserved in small GTPases (G domains, G1–G5, Figure 2, B–E, Supplemental Figure 1).²⁰ Ser76 is part of the G1 motif, also known as P-loop; Thr97 constitutes the G2 motif; and Pro119 resides in the G3 motif (Figure 2, B–E). These motifs are involved in the interaction with the phosphate moiety of the nucleotide. Ile221 resides in a sequence stretch corresponding to the G5 motif. The variants are expected to display low nucleotide affinity and fast nucleotide exchange. This may interfere with RagD-mediated signaling in different ways (please find a detailed description in the Supplemental Appendix 3). The mutations result in amino acid residues that are sterically more demanding and, at least in some cases, are incompatible with the fold observed in a crystal structure of human RagD (Protein Data Bank entry 2q3f), where switch I is folded over the nucleotide. Such a closed conformation is typically found in GTP- or GDP-bound small G proteins.²¹

RagD Is Expressed in the Distal Tubule of the Kidney

The mRNA expression of mouse *Rragd* was quantified in tissues of C57BL/6 mice and isolated DCT cells of parvalbumin-GFP mice by quantitative real-time PCR according to previously established methods.²² RagD showed a ubiquitous expression pattern with significant transcript levels in heart and kidney (Supplemental Figure 2A). Using primary antibodies against marker proteins for distal tubular segments—AQP2 for cortical collecting duct, NCC for the DCT, and UMOD for the TAL, as described previously¹⁷—RagD was shown to be colocalized with UMOD and NCC in the TAL and DCT nephron segments, respectively (Figure 3). Of note, mRNA expression of RagD

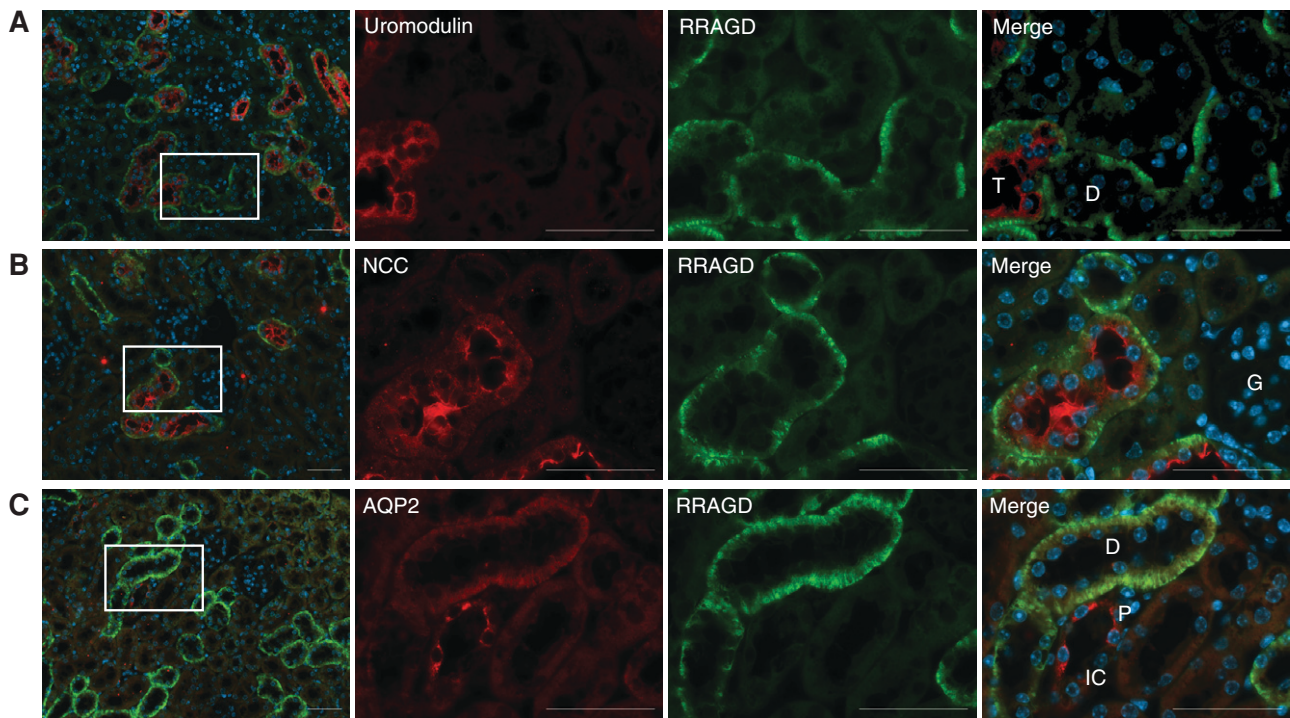


Figure 3. RagD is expressed in the DCT. (A–C) Double immunofluorescence staining of mouse kidney sections for RagD in green and (A) UMOD (red), (B) NCC (red), or (C) AQP2 (red). Bar, 50 μ m. D, distal tubule; G, glomerulus; IC, intercalated cell; P, principal cell; T, TAL.

was enriched in the DCT compared with total kidney (Supplemental Figure 2B). In contrast, RagD showed no colocalization with AQP2. These expression analyses confirm previous high-throughput quantitative transcriptomic and proteomic profiling data from microdissected rat kidney tubule segments.^{23,24} Additionally, single-cell RNA analyses of Ransick *et al.*²⁵ point to a strong expression of RagD in intercalated cells of the cortical and medullary collecting duct.

RagD Mutations Activate the mTOR Pathway

All RagD mutants showed increased binding to regulatory associated protein of mTOR (Raptor) and mTOR, the essential components of mTORC1 (Figure 4A), after exogenous expression in HEK293T cells. All human RagD mutants resulted in increased S6K1 phosphorylation in the presence of nutrients, indicative of active mTORC1 signaling. Of note, some mutants increased S6K1 phosphorylation even during starvation (Figure 4B).

To understand the molecular mechanisms of mTORC1 activation at the lysosomal membrane in an independent assay and to evaluate the effect of human RagD-p.Ser76Leu on mTORC1 complexes, we performed an unbiased

interactome analysis by label-free quantitative proteomics. For this purpose, FlpIn murine renal tubular epithelial cells expressing either a wt or mutant GFP.RagD-p.Ser75Leu fusion protein were subjected to immunoprecipitation of GFP.RagD and liquid chromatography with tandem mass spectrometry (Figure 4C). Using a hierarchic clustering of protein intensities from the dataset and applying stringent cutoff criteria, we identified 32 proteins that differentially coprecipitated with mRagD-p.Ser75Leu in comparison with wt RagD in seven independent experiments. Interestingly, mutant RagD-p.Ser75Leu showed a significantly increased coprecipitation of multiple proteins of the mTORC1 signaling complex at the lysosomal membrane (Figure 4D). These included the mTORC1 subunit Raptor and different subunits of lysosomal vacuolar-type H^+ -ATPase (V-ATPase, Atp6v-proteins). Additionally, proteins that tether the Rag GTPase dimer to the lysosomal surface were identified, such as members of the Lamtor protein family (Lamtor3, Lamtor5) and TMEM55B (Figure 4, C and D, Supplemental Figure 3). Of note, no major differences in expression or subcellular localization patterns were observed between the wt and the mutant fusion protein (Supplemental Figure 3).

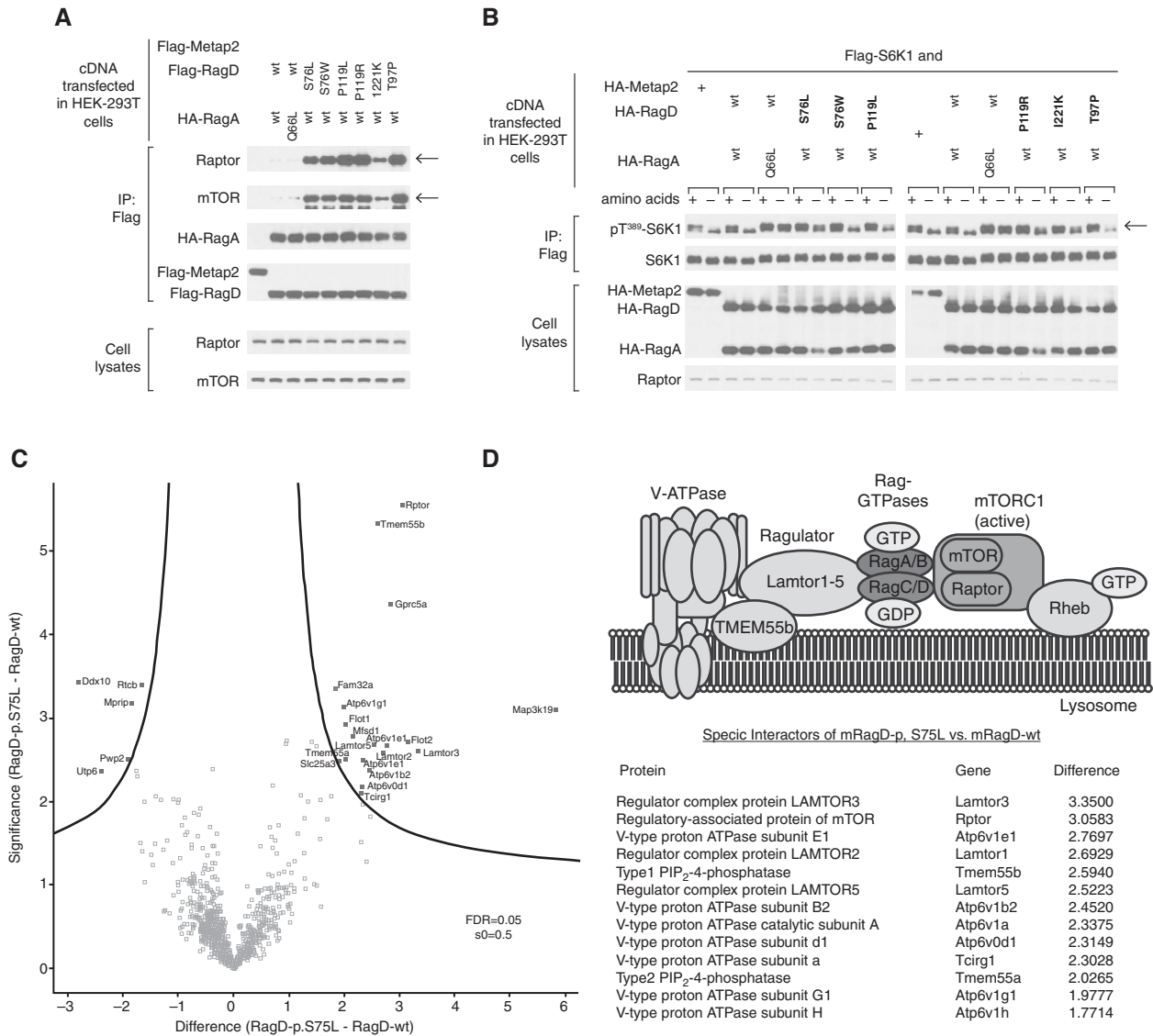


Figure 4. RRAGD mutations increase mTOR signaling *in vitro*. (A) Immunoblot analysis demonstrating that RagD mutations (bold) increase Raptor and mTOR binding (rows indicated by arrow). Hemagglutinin-RagA (HA-RagA) and FLAG-RagD blots indicate equal (co-)precipitation of the Rag dimer (middle rows). Transfected HEK293T cells contained equal amounts of Raptor and mTOR, as detected in the cell lysate fraction (bottom rows). Metap-2 (indicated by +) used as a negative control for nonspecific flag binding. (B) mTORC1 signaling in response to amino acids and starvation assessed by phosphorylation of its substrate S6 kinase (S6K1) at threonine 389 (Thr³⁸⁹), indicated by an arrow. Compared to wt RagD, all RagD mutants caused an increased S6K1 phosphorylation in the presence of amino acids. The expression of transfected RagA, RagD, and S6K1, and of endogenous Raptor, was confirmed by immunoblotting (bottom rows). Constitutively active RagA-p.Q66L served as a positive control.³⁴ Metap-2 (indicated by +) served as a negative control for nonspecific flag binding. (C) Volcano plot of the interactome of murine RagD-p.S75L versus RagD-wt. The significance (P value) of changes between RagD-p.S75L and RagD-wt (−log₁₀ scale) is plotted against the difference (fold change) between RagD-p.S75L and RagD-wt (log₂ scale). Dots beyond the curved line represent proteins with significantly increased abundance (false discovery rate [FDR], 0.05; s₀=0.5) in RagD-p.S75L samples (right) or RagD-wt samples (left). (D) Model of the V-ATPase-Ragulator-Rag-GTPase-mTORC1 complex and table listing the identified components from (C) that showed significantly increased binding to RagD-p.S75L in log₂ fold change. IP, immunoprecipitation.

DISCUSSION

This study describes a previously unrecognized hereditary disease phenotype combining an electrolyte-losing tubulopathy and DCM, which is caused by heterozygous missense variants in the *RRAGD* gene encoding Rag GTPase D. The identified *RRAGD* variants lead to increased mTOR signaling. We propose to call this novel inherited disease autosomal dominant kidney hypomagnesemia (ADKH-*RRAGD*).

The cardinal symptom of individuals with *RRAGD* mutations is a severe hypomagnesemia, resulting in muscle cramps, tetany, and cerebral seizures. Renal magnesium wasting was associated with hypercalciuria and nephrocalcinosis in a subset of individuals, a phenotype highly reminiscent of familial hypomagnesemia with hypercalciuria and nephrocalcinosis (FHHNC; Online Mendelian Inheritance in Man numbers 248250 and 248190).^{2,3} In FHHNC, mutations in two tight junction proteins, claudin-16 and claudin-19, cause a defective paracellular reabsorption of calcium and magnesium in the TAL.^{26–28} Indeed, immunostaining experiments showed RagD expression in the TAL, suggesting RagD variants may impair calcium ion and Mg²⁺ reabsorption in this tubular segment.

In a subset of patients, a renal phenotype with salt wasting and hypokalemic alkalosis prevailed, resembling Bartter syndrome. The prenatal finding of polyhydramnios in three individuals supported this assumption. Unfortunately, a systematic evaluation of the RAAS in our entire cohort was prevented by early cardiac insufficiency and treatment with diuretics and angiotensin-converting enzyme inhibitors. However, a marked activation of the RAAS was also noted in individual F2.1 years before cardiac manifestation, supporting the suspicion of a mixed FHHNC/salt-wasting phenotype. In contrast, hypercalciuria and nephrocalcinosis lacked in affected members of family F9. This phenotypic variability might be explained by a less pronounced activation of mTOR signaling by the RagD-p.T97P mutant, but could also reflect a primary dysfunction of the DCT with a Gitelman syndrome-like phenotype rather than a TAL defect. Similar observations have been made in Bartter syndrome type III due to *CLCNKB* defects, in which individuals might present with a phenotype ranging from antenatal Bartter syndrome to Gitelman syndrome.^{29,30} Future research will be required to elucidate the exact targets of increased mTOR signaling in distal tubular segments.

Besides the tubulopathy, present in all patients, DCM represented a serious clinical symptom leading to early heart failure and resulting in a heart transplantation in a substantial subset of patients. In fact, the impairment of cardiac function and the medical treatment with angiotensin-converting enzyme inhibitors and diuretics might have hampered the diagnosis of the tubulopathy in individual patients. Moreover, calcineurin inhibitor treatment might have aggravated hypomagnesemia in patients after cardiac transplantation.

Interestingly, the phenotype of our cohort is reminiscent of two individuals from a previously described Finnish family with unresolved renal tubular disease and cardiomyopathy.^{31,32} The clinical picture of these individuals is highly suggestive of ADKH-*RRAGD*. Unfortunately, the cardiac phenotype resulted in an early fatal issue in this family, which hampers any further genetic investigation.

RRAGD encodes a small Rag guanosine triphosphatase (GTPase), which is an essential component of the nutrient-sensing pathway that activates mTOR signaling.¹⁹ mTOR serves as the main nutrient sensor of the cell, coordinating signals from extracellular growth factors and intracellular nutrient availability, such as amino acids.^{15,33} mTOR forms the catalytic subunit of two distinct protein complexes, known as mTORC1 and mTORC2. Upon amino acid stimulation, Rag GTPases target mTORC1 to the lysosome where its kinase is activated.¹⁵ Indeed, our interaction studies demonstrate increased interaction of RagD-S76L to components of the mTOR signaling pathway and the Ragulator complex (Figure 4).

The function of the Rag GTPases depends on the differential binding of guanosine nucleotides.¹⁵ Engineered mutations that interfere with nucleotide binding were shown to critically affect Rag signaling and mTORC1 activation.³⁴ The human *RRAGD* mutations discovered in this study affect residues involved in the binding of guanosine nucleotides (Figure 2, B–D, Supplemental Figure 1). They lead to a constitutively increased activation of mTORC1, as reflected by an increased phosphorylation of its substrate S6K1 and by increased binding to components of the amino acid-sensing, mTORC1-containing complex (Figure 4). Previously, engineered mutations at the identical serine residue in RagC (p.Ser75Leu) and RagD (p.Ser76Leu) were shown to strongly interact with mTORC1, leading to constitutive mTOR pathway activation, irrespective of amino acid availability.¹⁵ Of note, when Rag subunits are highly overexpressed, some might become mislocalized and inappropriately encounter and activate mTORC1 in the absence of amino acids. How the individual mutations exactly affect GDP/GTP binding remains to be examined.

In a significant number of patients, *RRAGD* mutations resulted from *de novo* mutational events that are thought to originate either from errors in DNA replication or from inefficient repair of spontaneous DNA lesions.³⁵ The mutagenesis rate varies in different areas of the human genome, which is attributed to genome structure, but also to chromatin state and transcription rate. The occurrence of recurrent mutational events at identical positions (*i.e.*, *RRAGD* p.S76 or p.P119) suggests so-called mutational hotspots. An example are CpG dinucleotide sites facilitating C>T transitions.³⁶ Indeed, the *RRAGD* c.227C>T variant is located at such a CpG site, which may explain the recurrent mutation at RagD-p.S76.

Data on the role of mTOR signaling in tubular physiology remain scarce. Previous studies mainly focused on the

tubular effects of decreased mTORC1 signaling.^{37,38} Inactivation of mTOR signaling along the renal tubule was shown to lead either to a Fanconi-like syndrome or to a urine-concentrating defect attributed to impaired distal tubular transport processes.³⁹ Remarkably, hypomagnesemia and hypokalemia have been observed in rats after sirolimus treatment that were attributed to GSH expression of NKCC2 (*SLC12A1*) in the TAL.⁴⁰ Moreover, inhibition of mTOR signaling also resulted in changes in TRPM6 expression in the DCT.⁴¹ Conversely, mTORC1 activation by knockout of *Tsc1* in renal tubular cells resulted in cyst formation resembling polycystic kidney disease.^{42,43} The role of mTORC1 in cyst formation depends on its downstream target S6K1.⁴⁴ Other mTORC1 targets, including autophagy mutants and 4E-BP1/4E-BP2, do not recapitulate a polycystic kidney phenotype.^{45,46} Therefore, follow-up studies will be needed to identify the precise roles of RagD and mTORC1 signaling in the distal tubular handling of electrolytes.

Although the molecular pathways downstream of mTOR in the TAL and DCT remain to be determined, mTORC2 has been demonstrated to regulate the aldosterone-sensitive epithelial sodium channel in the collecting duct.^{47,48} mTORC2 activates serum and glucocorticoid inducible kinase 1 (SGK1), resulting in increased cell surface expression of the epithelial sodium channel. However, it should be noted that the RAG complex specifically activates mTORC1.

The finding of DCM in a subset of our patients also substantiates a critical role of Rag GTPases for cardiac function. Previously, inactivation of Rag GTPases RagA and RagB was shown to result in hypertrophic cardiomyopathy in mice.⁴⁹ Moreover, a *de novo* mutation in RagC (p.Ser75Tyr), leading to increased mTOR activity, has been described in an individual with DCM.⁵⁰ Recent studies in clinical and experimental models of DCM have implicated mTOR hyperactivation as a major cause of DCM.^{51,52} In line with this, inhibition of mTOR by rapamycin has been demonstrated to successfully improve cardiac function in animal models of DCM.^{53–55} Of note, not all identified *RRAGD* mutations overactivated mTORC1 signaling equally. Our experiments indicate that p.Thr97Pro results in less S6K1 activation (Figure 4), which may explain why individuals carrying this mutation do not suffer from DCM even at adult age. A targeted treatment of increased mTOR activity in patients with *RRAGD* mutations will represent an appealing therapeutic strategy in the future.

Taken together, the discovery of *RRAGD* mutations establishes a novel hereditary tubulopathy linked to dysregulation of the mTOR pathway. The diagnosis of ADKH-*RRAGD* should be considered in individuals presenting either with early-onset DCM and/or hypomagnesemia of renal origin. Future research will hopefully help to enlighten the exact role of mTOR for distal tubular

transport processes and renal magnesium handling in particular.

DISCLOSURES

B.B. Beck reports receiving honoraria from Alnylam and Oxthera; and serving as a scientific advisor for, or member of, the Oxalosis and Hyperoxaluria Foundation. C. Bergmann reports receiving honoraria from Alexion, Atheneum, Kyowa Kirin, Merck, Otsuka, PTC, and Sanofi; serving on the on the advisory boards for Alexion and PTC, and on the medical and scientific board of the German PKD Foundation; having other interests in/relationships with American Society of Nephrology, Deutsche Gesellschaft für Nephrologie (DGfN), European Renal Association–European Dialysis and Transplant Association (ERA-EDTA), European Society for Paediatric Nephrology, German Pediatric Nephrology Association (GPN), and International Pediatric Nephrology Association, as a member of the kidney community; receiving research funding from Limbach; having ownership interest in Medizinische Genetik Mainz; and being employed by Medizinische Genetik Mainz, Limbach Genetics. A. Braun reports receiving research funding from the Köln Fortune Grant (Faculty of Medicine, University of Cologne). S. Burtey reports receiving honoraria from AstraZeneca, Fresenius Kabi, Gambro, and Nipro. K. Dahan reports serving as president and a member of the advisory committees for the nonprofit patient organizations Association for Information and research on Renal Genetic diseases (AIRG), Familial Adenomatous Polyposis Association (FAPA), and Retina; receiving research funding from Alexion, Alnylam, IPSEN, MSD, Pfizer, Servier, and Sobi; and serving on the board of directors of the Institute for Pathology and Genetics (IPG). P. Houillier reports having consultancy agreements with Amgen, Kyowa Kirin, and Shire/Takeda; receiving research funding from Amgen and Takeda/Shire; having other interests in/relationships with the European Society of Endocrinology *via* a working group on calcium and bone; serving as a member of the editorial board for *JASN*; receiving honoraria from Kyowa Kirin and Takeda/Shire; and serving as a scientific advisor for the National Centre of Competence in Research (NCCR) Kidney.CH (Switzerland). F. Jouret reports serving as a scientific advisor for, or member of, the Belgian Society of Nephrology and the French-speaking Society of Transplantation. N.V.A.M. Knoers reports serving as chair of the ERA-EDTA Working Group on Inherited Kidney Diseases, and chair of the Molecular Diagnostics Task Force for the European Rare Kidney Disease Reference Network; receiving honoraria from ErasmusMC, The Netherlands, for Strategy Evaluation Protocol (SEP) evaluation; and serving as a scientific advisor or member of different research advisory committees without any financial compensation. M. Konrad reports having consultancy agreements with Otsuka. M. C. Liebau reports serving on editorial boards for *Current Pediatric Reviews*, *Frontiers in Pediatrics*, and *Pediatric Nephrology*; serving on the council for the European Society for Paediatric Nephrology, on the scientific committee of the German PKD Foundation, on a scientific advisory committee for the PKD Foundation; having consultancy agreements with Otsuka Pharma as a member of an advisory board representing the University Hospital of Cologne; receiving honoraria from Pfizer. J. Oh reports having consultancy agreements with, and receiving honoraria from, Alexion, Alnylam, Amgen, Boehringer Ingelheim, Chiesi, Horizon, Novartis, Recordati, and Sanofi; receiving research funding from Amgen, Chiesi, Novartis, and Sanofi; and serving as a scientific advisor for, or member of, *Pediatric Nephrology*. D. Sabatini reports serving as a scientific advisory board member of Atavistik Bio Inc., Faeth Therapeutics Inc., Montai Health (f/k/a FL65), Navitor, Toran Pharmaceuticals (f/k/a VL54), and Vescor Therapeutics. K. Shen reports receiving research funding from National Institutes of Health/National Cancer Institute (grant K22CA241362). R. Vargas-Poussou reports serving as a scientific advisor for, or member of, Advicenne. All remaining authors have nothing to disclose.

FUNDING

This work was supported by the Nederlandse Organisatie voor Wetenschappelijk Onderzoek (Netherlands Organization for Scientific Research) grant NWO VENI 016.186.012, Diabetes Fonds (Dutch Diabetes Research Foundation) grant 2017.81.014, Nierstichting (Dutch Kidney Foundation) grant 15OKG18 (to K.Y. Renkema), and the European Union Seventh Framework Programme EUREnOmics project FP7/2007-2013, number 305608. F. Jouret is a Fellow of the Fonds National de la Recherche Scientifique in Belgium. This work was financially supported by the IMAGEN project which is co-funded by the PPP Allowance made available by Health~Holland, Top Sector Life Sciences & Health, to stimulate public-private partnerships (Implementation of Advancements in GENetic Kidney Disease, LSHM20009) and the Dutch Kidney Foundation (20OP+018). Additionally, we received support from ZonMW under the frame of EJPRD, the European Joint Programme on Rare Diseases (EJPRD2019-40).

ACKNOWLEDGMENTS

The authors are grateful to the patients for their participation in this study. We thank Ms. Edith Peters, Ms. Femke Latta, Miss Valentina Carotti, Mr. Ruud Tilleman, Mr. Matthijs Snelders, Ms. Laurence Poma, and Ms. Ruth Herzog for their excellent technical support, and Dr. Tanja Seidel for thoughtful patient care.

SUPPLEMENTAL MATERIAL

This article contains the following supplemental material online at <https://jasn.asnjournals.org/lookup/suppl/doi:10.1681/ASN.2021030333/-/DCSupplemental>.

Supplemental Appendix 1. Complete methods.

Supplemental Appendix 2. Detailed clinical description of affected individuals.

Supplemental Appendix 3. Detailed description of the structural consequences of the mutations.

Supplemental Appendix 4. References.

Supplemental Table 1. Biochemical parameters F9.

Supplemental Figure 1. RagD mutations affect conserved residues.

Supplemental Figure 2. Tissue expression of RagD.

Supplemental Figure 3. Analysis of the RagD interactome.

REFERENCES

- Downie ML, Lopez Garcia SC, Kleta R, Bockenhauer D: Inherited tubulopathies of the kidney: Insights from genetics. *Clin J Am Soc Nephrol* 16: 620–630, 2021
- Viering DHHM, de Baaij JHF, Walsh SB, Kleta R, Bockenhauer D: Genetic causes of hypomagnesemia, a clinical overview. *Pediatr Nephrol* 32: 1123–1135, 2017
- de Baaij JHF, Hoenderop JGJ, Bindels RJM: Magnesium in man: Implications for health and disease. *Physiol Rev* 95: 1–46, 2015
- Hou J, Renigunta A, Gomes AS, Hou M, Paul DL, Waldegger S, et al.: Claudin-16 and claudin-19 interaction is required for their assembly into tight junctions and for renal reabsorption of magnesium. *Proc Natl Acad Sci USA* 106: 15350–15355, 2009
- Gong Y, Renigunta V, Himmerkus N, Zhang J, Renigunta A, Bleich M, et al.: Claudin-14 regulates renal Ca⁺⁺ transport in response to CaSR signalling via a novel microRNA pathway. *Embo J* 31: 1999–2012, 2012
- Mittermeier L, Demirkhanyan L, Stadlbauer B, Breit A, Recordati C, Hilgendorff A, et al.: TRPM7 is the central gatekeeper of intestinal mineral absorption essential for postnatal survival. *Proc Natl Acad Sci USA* 116: 4706–4715, 2019
- Schäffers OJM, Hoenderop JGJ, Bindels RJM, de Baaij JHF: The rise and fall of novel renal magnesium transporters. *Am J Physiol Renal Physiol* 314: F1027–F1033, 2018
- Schlingmann KP, Weber S, Peters M, Niemann Nejsum L, Vitzthum H, Klingel K, et al.: Hypomagnesemia with secondary hypocalcemia is caused by mutations in TRPM6, a new member of the TRPM gene family. *Nat Genet* 31: 166–170, 2002
- de Baaij JH, Blanchard MG, Lavrijsen M, Leipziger J, Bindels RJ, Hoenderop JG: P2X4 receptor regulation of transient receptor potential melastatin type 6 (TRPM6) Mg²⁺ channels. *Pflugers Arch* 466: 1941–1952, 2014
- Feroli S, Zierler S, Zaißerer J, Schredelseker J, Gudermann T, Chubanov V: TRPM6 and TRPM7 differentially contribute to the relief of heteromeric TRPM6/7 channels from inhibition by cytosolic Mg²⁺ and Mg-ATP. *Sci Rep* 7: 8806, 2017
- Nair AV, Hocher B, Verkaart S, van Zeeland F, Pfab T, Slowinski T, et al.: Loss of insulin-induced activation of TRPM6 magnesium channels results in impaired glucose tolerance during pregnancy. *Proc Natl Acad Sci USA* 109: 11324–11329, 2012
- Thebault S, Alexander RT, Tiel Groenestege WM, Hoenderop JG, Bindels RJ: EGF increases TRPM6 activity and surface expression. *J Am Soc Nephrol* 20: 78–85, 2009
- Altmüller J, Motameny S, Becker C, Thiele H, Chatterjee S, Wollnik B, et al.: A systematic comparison of two new releases of exome sequencing products: The aim of use determines the choice of product. *Biol Chem* 397: 791–801, 2016
- Hart SN, Duffy P, Quest DJ, Hossain A, Meiners MA, Kocher JP: VCF-Miner: GUI-based application for mining variants and annotations stored in VCF files. *Brief Bioinform* 17: 346–351, 2016
- Sancak Y, Peterson TR, Shaul YD, Lindquist RA, Thoreen CC, Bar-Peled L, et al.: The rag GTPases bind raptor and mediate amino acid signaling to mTORC1. *Science* 320: 1496–1501, 2008
- Dafinger C, Rinschen MM, Borgal L, Ehrenberg C, Basten SG, Franke M, et al.: Targeted deletion of the AAA-ATPase Ruvbl1 in mice disrupts ciliary integrity and causes renal disease and hydrocephalus. *Exp Mol Med* 50: 1–17, 2018
- Kurstjens S, Smeets B, Overmars-Bos C, Dijkman HB, den Braanker DJW, de Bel T, et al.: Renal phospholipidosis and impaired magnesium handling in high-fat-diet-fed mice. *FASEB J* 33: 7192–7201, 2019
- Walsh PR, Tse Y, Ashton E, Iancu D, Jenkins L, Bienias M, et al.: Clinical and diagnostic features of bartter and gitelman syndromes. *Clin Kidney J* 11: 302–309, 2018
- Saxton RA, Sabatini DM: mTOR signaling in growth, metabolism, and disease. *Cell* 168: 960–976, 2017
- Nicastro R, Sardu A, Panchoaud N, De Virgilio C: The architecture of the rag GTPase signaling network. *Biomolecules* 7: 48, 2017
- Vetter IR, Wittinghofer A: The guanine nucleotide-binding switch in three dimensions. *Science* 294: 1299–1304, 2001
- de Baaij JHF, Stuiver M, Meij IC, Lainez S, Kopplin K, Venselaar H, et al.: Membrane topology and intracellular processing of cyclin M2 (CNNM2). *J Biol Chem* 287: 13644–13655, 2012
- Lee JW, Chou CL, Knepper MA: Deep sequencing in microdissected renal tubules identifies nephron segment-specific transcriptomes. *J Am Soc Nephrol* 26: 2669–2677, 2015
- Limbutara K, Chou CL, Knepper MA: Quantitative proteomics of all 14 renal tubule segments in rat. *J Am Soc Nephrol* 31: 1255–1266, 2020
- Ransick A, Lindström NO, Liu J, Zhu Q, Guo JJ, Alvarado GF, et al.: Single-cell profiling reveals sex, lineage, and regional diversity in the mouse kidney. *Dev Cell* 51: 399–413.e7, 2019
- Konrad M, Schaller A, Seelow D, Pandey AV, Waldegger S, Lesslauer A, et al.: Mutations in the tight-junction gene claudin 19 (CLDN19) are associated with renal magnesium wasting, renal failure, and severe ocular involvement. *Am J Hum Genet* 79: 949–957, 2006

27. Simon DB, Lu Y, Choate KA, Velazquez H, Al-Sabban E, Praga M, et al.: Paracellin-1, a renal tight junction protein required for paracellular Mg²⁺ resorption. *Science* 285: 103–106, 1999
28. Hanssen O, Castermans E, Bovy C, Weekers L, Ercicum P, Dubois B, et al.: Two novel mutations of the CLDN16 gene cause familial hypomagnesaemia with hypercalciuria and nephrocalcinosis. *Clin Kidney J* 7: 282–285, 2014
29. Jeck N, Konrad M, Peters M, Weber S, Bonzel KE, Seyberth HW: Mutations in the chloride channel gene, CLCNKB, leading to a mixed Bartter-Gitelman phenotype. *Pediatr Res* 48: 754–758, 2000
30. Zelikovic I, Szargel R, Hawash A, Labay V, Hatib I, Cohen N, et al.: A novel mutation in the chloride channel gene, CLCNKB, as a cause of Gitelman and Bartter syndromes. *Kidney Int* 63: 24–32, 2003
31. Laine J, Jalanko H, Alakulppi N, Holmberg C: A new tubular disorder with hypokalaemic metabolic alkalosis, severe hypermagnesuric hypomagnesaemia, hypercalciuria and cardiomyopathy. *Nephrol Dial Transplant* 20: 1241–1245, 2005
32. Runeberg L, Collan Y, Jokinen EJ, Lähdevirta J, Aro A: Hypomagnesemia due to renal disease of unknown etiology. *Am J Med* 59: 873–881, 1975
33. Shimobayashi M, Hall MN: Making new contacts: The mTOR network in metabolism and signalling crosstalk. *Nat Rev Mol Cell Biol* 15: 155–162, 2014
34. Shen K, Choe A, Sabatini DM: Intersubunit crosstalk in the rag GTPase heterodimer enables mTORC1 to respond rapidly to amino acid availability. *Mol Cell* 68: 821, 2017
35. Maki H: Origins of spontaneous mutations: Specificity and directionality of base-substitution, frameshift, and sequence-substitution mutageneses. *Annu Rev Genet* 36: 279–303, 2002
36. Acuna-Hidalgo R, Veltman JA, Hoischen A: New insights into the generation and role of de novo mutations in health and disease. *Genome Biol* 17: 241, 2016
37. Grahammer F, Haenisch N, Steinhardt F, Sandner L, Roerden M, Arnold F, et al.: mTORC1 maintains renal tubular homeostasis and is essential in response to ischemic stress. *Proc Natl Acad Sci USA* 111: E2817–E2826, 2014
38. Grahammer F, Wanner N, Huber TB: mTOR controls kidney epithelia in health and disease. *Nephrol Dial Transplant* 29: i9–i18, 2014
39. Grahammer F, Ramakrishnan SK, Rinschen MM, Larionov AA, Syed M, Khatib H, et al.: mTOR regulates endocytosis and nutrient transport in proximal tubular cells. *J Am Soc Nephrol* 28: 230–241, 2017
40. da Silva CA, de Bragança AC, Shimizu MH, Sanches TR, Fortes MA, Giorgi RR, et al.: Rosiglitazone prevents sirolimus-induced hypomagnesemia, hypokalemia, and downregulation of NKCC2 protein expression. *Am J Physiol Renal Physiol* 297: F916–F922, 2009
41. Ikari A, Sanada A, Sawada H, Okude C, Tonegawa C, Sugatani J: Decrease in transient receptor potential melastatin 6 mRNA stability caused by rapamycin in renal tubular epithelial cells. *Biochim Biophys Acta* 1808: 1502–1508, 2011
42. Centini R, Tsang M, Iwata T, Park H, Delrow J, Margineantu D, et al.: Loss of Fnip1 alters kidney developmental transcriptional program and synergizes with TSC1 loss to promote mTORC1 activation and renal cyst formation. *PLoS One* 13: e0197973, 2018
43. Zhou J, Brugarolas J, Parada LF: Loss of Tsc1, but not Pten, in renal tubular cells causes polycystic kidney disease by activating mTORC1. *Hum Mol Genet* 18: 4428–4441, 2009
44. Bonucci M, Kuperwasser N, Barbe S, Koka V, de Villeneuve D, Zhang C, et al.: mTOR and S6K1 drive polycystic kidney by the control of Afadin-dependent oriented cell division. *Nat Commun* 11: 3200, 2020
45. Le Bacquer O, Combe K, Patrac V, Ingram B, Combaret L, Dardevet D, et al.: 4E-BP1 and 4E-BP2 double knockout mice are protected from aging-associated sarcopenia. *J Cachexia Sarcopenia Muscle* 10: 696–709, 2019
46. Orhon I, Dupont N, Zaidan M, Boitez V, Burtin M, Schmitt A, et al.: Primary-cilium-dependent autophagy controls epithelial cell volume in response to fluid flow. *Nat Cell Biol* 18: 657–667, 2016
47. Gleason CE, Frindt G, Cheng CJ, Ng M, Kidwai A, Rashmi P, et al.: mTORC2 regulates renal tubule sodium uptake by promoting ENaC activity. *J Clin Invest* 125: 117–128, 2015
48. Lu M, Wang J, Jones KT, Ives HE, Feldman ME, Yao LJ, et al.: mTOR complex-2 activates ENaC by phosphorylating SGK1. *J Am Soc Nephrol* 21: 811–818, 2010
49. Kim YC, Park HW, Sciarretta S, Mo JS, Jewell JL, Russell RC, et al.: Rag GTPases are cardioprotective by regulating lysosomal function. *Nat Commun* 5: 4241, 2014
50. Long PA, Zimmermann MT, Kim M, Evans JM, Xu X, Olson TM: De novo RRAGC mutation activates mTORC1 signaling in syndromic fetal dilated cardiomyopathy. *Hum Genet* 135: 909–917, 2016
51. Caragnano A, Aleksova A, Bulfoni M, Cervellin C, Rolle IG, Veneziano C, et al.: Autophagy and inflammasome activation in dilated cardiomyopathy. *J Clin Med* 8: 1519, 2019
52. Jin B, Shi H, Zhu J, Wu B, Geshang Q: Up-regulating autophagy by targeting the mTOR-4EBP1 pathway: A possible mechanism for improving cardiac function in mice with experimental dilated cardiomyopathy. *BMC Cardiovasc Disord* 20: 56, 2020
53. Choi JC, Worman HJ: Reactivation of autophagy ameliorates LMNA cardiomyopathy. *Autophagy* 9: 110–111, 2013
54. Marin TM, Keith K, Davies B, Conner DA, Guha P, Kalaitzidis D, et al.: Rapamycin reverses hypertrophic cardiomyopathy in a mouse model of LEOPARD syndrome-associated PTPN11 mutation. *J Clin Invest* 121: 1026–1043, 2011
55. Ramos FJ, Chen SC, Garelick MG, Dai DF, Liao CY, Schreiber KH, et al.: Rapamycin reverses elevated mTORC1 signaling in lamin A/C-deficient mice, rescues cardiac and skeletal muscle function, and extends survival. *Sci Transl Med* 4: 144ra103, 2012
56. Hoyer PF: Nephrocalcinosis. In: *Ultraschalldiagnostik in Pädiatrie Und Kinderchirurgie: Lehrbuch und Atlas*, edited by Deeg KH, Hofmann V, and Hoyer PF, Stuttgart, Germany, Thieme, 1996, pp 372–374
57. Pettersen MD, Du W, Skeens ME, Humes RA: Regression equations for calculation of z scores of cardiac structures in a large cohort of healthy infants, children, and adolescents: An echocardiographic study. *J Am Soc Echocardiogr* 21: 922–934, 2008

AFFILIATIONS

¹Department of General Pediatrics, University Children's Hospital, Münster, Germany

²Division of Nephrology, Department of Internal Medicine, University of Liège Hospital, Liège, Belgium

³Interdisciplinary Group of Applied Genoproteomics, Cardiovascular Sciences, University of Liège, Liège, Belgium

⁴Whitehead Institute for Biomedical Research, Cambridge, Massachusetts

⁵Department of Biology, Howard Hughes Medical Institute, Massachusetts Institute of Technology, Cambridge, Massachusetts

⁶Koch Institute for Integrative Cancer Research, Cambridge, Massachusetts

⁷Broad Institute of Harvard and Massachusetts Institute of Technology, Cambridge, Massachusetts

- ⁸Program in Molecular Medicine, University of Massachusetts Medical School, Worcester, Massachusetts
- ⁹Department of Genetics, Center for Molecular Medicine, University Medical Center Utrecht, Utrecht University, Utrecht, The Netherlands
- ¹⁰Department of Physiology, Radboud Institute for Molecular Life Sciences, Radboud University Medical Center, Nijmegen, The Netherlands
- ¹¹Department of Pediatrics and Center for Molecular Medicine Cologne, Faculty of Medicine, University of Cologne and University Hospital Cologne, Cologne, Germany
- ¹²Department II of Internal Medicine and Center for Molecular Medicine Cologne, Faculty of Medicine, University of Cologne and University Hospital Cologne, Cologne, Germany
- ¹³Cordeliers Research Center, Centre National de la Recherche Scientifique (CNRS), ERL8228, Institut National de la Santé et de la Recherche Médicale (INSERM), Sorbonne University, University of Paris, Paris, France
- ¹⁴Department of Physiology, Assistance Publique-Hôpitaux de Paris (AP-HP), European Hospital Georges Pompidou, Paris, France
- ¹⁵Reference Center for Hereditary Renal Diseases in Children and Adults (MARHEA), Paris, France
- ¹⁶Department of Pediatrics, Vanderbilt University Medical Center, Nashville, Tennessee
- ¹⁷Department of Pediatric Cardiology, University Children's Hospital, Münster, Germany
- ¹⁸Department of Pediatrics, University Medical Center Hamburg-Eppendorf, Hamburg, Germany
- ¹⁹Division of Pediatric Nephrology, Saint-Luc University Clinics, Catholic University of Louvain, Brussels, Belgium
- ²⁰Department of Pediatric Endocrinology and Diabetes, School of Medicine, Marmara University, Istanbul, Turkey
- ²¹Center for Nephrology and Renal Transplantation, Assistance Publique-Hôpitaux de Marseille, Aix-Marseille University, Marseille, France
- ²²Division of Nephrology-Dialysis, Department of Internal Medicine, CHR Verviers East Belgium, Verviers, Belgium
- ²³Department of Molecular Cancer Research, Center for Molecular Medicine, Onco Institute, University Medical Center Utrecht, Utrecht, The Netherlands
- ²⁴Cardiopathology, Institute for Pathology and Neuropathology, University Hospital Tübingen, Tübingen, Germany
- ²⁵Institute for Genetics of Heart Diseases (IfGH), Department of Cardiovascular Medicine, University Hospital Münster, Münster, Germany
- ²⁶CECAD, Faculty of Medicine, University of Cologne and University Hospital Cologne, Cologne, Germany
- ²⁷Limbach Genetics, Medizinische Genetik Mainz, Mainz, Germany
- ²⁸Division of Nephrology, Department of Medicine, University Hospital Freiburg, Breisgau, Germany
- ²⁹Cologne Center for Genomics, University of Cologne, Cologne, Germany
- ³⁰Institute of Human Genetics, University Hospital Cologne and University of Cologne, Faculty of Medicine, Cologne, Germany
- ³¹Center for Molecular Medicine Cologne, University of Cologne, Faculty of Medicine, University Hospital Cologne, Cologne, Germany
- ³²Center of Human Genetics, Gosselies, Belgium
- ³³Division of Nephrology, Saint-Luc University Clinics, Catholic University of Louvain, Brussels, Belgium
- ³⁴Department of Genetics, AP-HP, European Hospital Georges Pompidou, Paris, France
- ³⁵Department of Genetics, University Medical Center Groningen, University of Groningen, Groningen, The Netherlands
- ³⁶Center for Rare Diseases, Medical Faculty, University of Cologne and University Hospital Cologne, Cologne, Germany

SUPPLEMENTAL DATA

Text

1. Complete methods
2. Detailed clinical description of affected individuals
3. Detailed description of the structural consequences of the mutations
4. References

Tables

1. Biochemical parameters F9

Figures

1. RagD mutations affect conserved residues
2. Tissue expression of RagD
3. Analysis of the RagD interactome

COMPLETE METHODS

Whole Exome Sequencing

Genomic DNA was extracted from EDTA blood according to standard procedures. Individuals F1.1, F2.1, F3.1, F4.1 F7.1 and F8.1 were subjected to whole exome sequencing as described previously.¹ In short, we used a customized sequence capture library that targeted exons and additional 35 bp of flanking intronic sequence. Genomic DNA was fragmented, and the coding exons as well as the corresponding exon-intron boundaries were enriched using the Roche/NimbleGen sequence capture approach (NimbleGen, Madison, Wisconsin, USA). They were then amplified and sequenced simultaneously by Illumina next generation sequencing (NGS) technology using an Illumina NextSeq system. NGS data analysis was performed by mapping paired end reads (2×100 bp) from the NextSeq instrument against the hg19 human reference genome using BWA with recommended standard settings. Mapped reads were preprocessed with SAM tools and duplicate reads were marked by Picard. Finally, GATK was applied for local realignment and base quality score recalibration of mapped reads. Filtering steps excluded common SNPs (> 1%), introns, untranslated regions (UTR), synonymous variants and low-coverage regions (< 5 reads). Overlaps of the remaining variants were generated using VCFMiner to select genes that were present in F1.1-F4.1 using the following settings: non-synonymous variants in exons and canonical splice sites, with a minor allele frequency from Exac, and in house data of less than 1%. This analysis resulted in the identification of 1 remaining gene *RRAGD*.² Subsequently, patients F5.1 and F6.1 were subjected to Sanger sequencing of the complete *RRAGD* gene.

Whole Genome Sequencing (WGS) in family 9

Genomic DNA was extracted from 10 ml EDTA blood according to standard and automated procedures. DNA samples of family 9, members III.1, III.6, and IV.2, were subjected to WGS on the Illumina X Ten platform (Hartwig Medical Foundation Amsterdam, The Netherlands). WGS

reads were processed by following the Genome Analysis ToolKit (GATK) best practices guidelines¹ where FASTQC was applied for quality control of the raw data. Sequencing reads were mapped onto the human genome (GRCh37/hg19) using Burrows Wheeler Aligner (v.0.7.5a). As part of GATK best practices, duplicate reads were removed with Picard (v.1.119), VariantRecalibrator was used for recalibration of base quality scores, and single nucleotide variants (SNVs) and indels were called using HaplotypeCaller (v.3.2-2). Next, copy number variants were called using FreeC (v.10.4) and structural variants were called using Delly (v.0.7.2) and Manta (v.1.0.3). The variants called were further prioritized and classified using Agilent Cartagenia software (v.4.3.5) based on the American College of Medical Genetics (ACMG) guidelines on SNV interpretation², population frequency (Minor Allele Frequency; MAF < 0.0001) acquired from the 1000 Genomes Phase 1 & 3, Exome Aggregation Consortium (ExAC) and the Genome of The Netherlands (GoNL v.5), location of the variants (exonic, 5' untranslated region, 3' untranslated region, intronic regions limited to 20 base pairs upstream and downstream of exons, and non-coding RNA exonic regions), variant quality (read depth \geq 10 and filter status = PASS), conservation scores, and *in silico* predicted effects on gene products and functions (SIFT \leq 0.5, PolyPhen-2 HumDiv = possibly or probably damaging, PolyPhen-2 HumVar = possibly or probably damaging, Mutation Taster = disease-causing, and FATHMM \leq 0). Final fine-tuning filtering steps involved overlap of variants in family members III.1, III.6, IV.2 and determination of the novelty of overlapping variants identified, (MAF = 0; using Genome Aggregation Database; <https://gnomad.broadinstitute.org/>), exploring literature and databases on known biological information from sources such as Online Mendelian Inheritance in Man (<https://www.omim.org/>) and The Human Protein Atlas (<https://www.proteinatlas.org>). Three overlapping heterozygous variants among the three patients were confirmed and checked for co-segregation in the family by Sanger sequencing (Macrogen®, Amsterdam, The Netherlands).

Linkage in family 9

Parametric linkage was performed using the MLINK program from the FASTLINK package version 4.1p assuming full penetrance, no phenocopies, and a disease frequency and population frequency of the mutation of 1 / 10,000.^{3,4}

Next generation sequencing for the detection of maternal mosaicism in family 7

We used a customized sequence capture library [Lu et al., 2017] that targeted exons and additional 35 bp of flanking intronic sequence. Genomic DNA was fragmented, and the coding exons as well as the corresponding exon-intron boundaries were enriched using the Roche/NimbleGen sequence capture approach (NimbleGen, Madison, Wisconsin, USA). They were then amplified and sequenced simultaneously by Illumina next generation sequencing (NGS) technology using an Illumina NextSeq system. NGS data analysis was performed by mapping paired end reads (2×100 bp) from the NextSeq instrument against the hg19 human reference genome using Burrows Wheeler Aligner with recommended standard settings. Mapped reads were preprocessed with SAM (Sequence Alignment/Map) tools and duplicate reads were marked by Picard. Finally, the Genome Analysis ToolKit (GATK) was applied for local realignment and base quality score recalibration of mapped reads. JSI Medical Systems software (version 4.1.2, SeqNext module) was used for visualization.

Cell culture and transfection

HEK293T cells were obtained from ATCC and maintained in an incubator set at 37°C and 5% CO₂. HEK293T cells were cultured in DMEM with 10% (v/v) FBS supplemented with 2 mM glutamine, penicillin (100 IU/ml), and streptomycin (100 mg/ml). For co-transfection experiments, 2,000,000 HEK-293T cells were plated in 10 cm culture dishes. Twenty-four hours later, cells were transfected using Xtremegene 9 transfection reagent with the pRK5-based cDNA expression plasmids indicated in the figures.

For stable expression of a GFP-GFP, GFP-RagD-wt or GFP-RagD-p.Ser75Leu fusion protein FlpIn IMCD cells were transfected with the pGLAP3 vector containing murine *Rragd* (WT or Ser75Leu) or GFP CDS, respectively, and Flp-recombinase expression vector (pOG44, Invitrogen) using Lipofectamine 2000 (Invitrogen). Stably integrated cells were selected by Hygromycin B (Invivogen) treatment.

Cell Lysates and Immunoprecipitation

To determine the response of mTORC1 to amino acid stimulation or starvation under the control of Rag mutants, two million HEK293T cells were plated onto a 10-cm dish. Twenty-four hours later, the cells were transfected with 2 ng of S6K1 and 100 ng of each Rag wildtype or mutant construct. Thirty-six hours later, amino acid stimulation or starvation was performed for 0.5-1 hour. Cells were rinsed once with ice-cold PBS and lysed with Triton lysis buffer (40 mM Na-HEPES, pH 7.4; 5 mM MgCl₂; 100 mM ATP; 10 mM Na₄P₂O₇; 10 mM Na β-glycerol phosphate; 1% v/v Triton; and one tablet of protease inhibitor cocktail per 25 mL of buffer). The lysates were cleared by centrifugation at 15,000 rpm at 4°C in a microcentrifuge for 10 minutes. For immunoprecipitations, the FLAGM2 beads were pre-equilibrated in Triton lysis buffer. 30 μL of a 50/50 slurry of the FLAG-M2 affinity beads were then added to cleared lysates and incubated at 4°C for two hours. Following immunoprecipitation, the beads were washed one time with Triton lysis buffer and 3 times with Triton lysis buffer supplemented with 500 mM NaCl. Immunoprecipitated proteins were denatured by the addition of 50 μL of 2.5 x SDS buffer, resolved by SDS-PAGE, and analyzed by immunoblotting.

Sample preparation for interactome analysis

FlpIn IMCD cells expressing a single copy of GFP-GFP, GFP-RagD-wt or GFP-RagD-Ser75Leu fusion proteins were lysed in lysis buffer (1% Triton X-100, 20 mM Tris pH 7.5, 25 mM NaCl, 50

mM NaF, 15 mM Na₄P₂O₇, 1 mM EDTA, 1xPIM, and 5 mM Na₃VO₄) and by sonication (30% amplitude, 9 s, 0.1 s sonic, 0.9 s pause). Lysates were cleared by centrifugation (17,000 g, 15 min, 4°C), followed by incubation with GFP μ MACS magnetic beads (Miltenyi) for 1 h. Then, lysates were loaded on a μ MACS column and precipitated proteins were reduced, alkylated and on-column digestion was performed over-night as previously described.⁵ Eluates were acidified the next day using 1-2% formic acid and stage-tip clean-up was performed as previously described and samples were dried using a vacuum centrifuge.⁶

nLC-MS/MS

Peptides were resuspended in 0.1% FA and were separated using a 1h gradient on an nLC coupled to a Q Exactive Plus tandem mass spectrometer (Thermo scientific) or an LTQ orbitrap XL mass spectrometer. Separation was carried out on an in-house packed 50 cm column with 1.7 μ m C18 beads (Dr Maisch GmbH). The gradient consisted of two buffers, Buffer A: 0.1% formic acid and B: 80% acetonitrile, 0.1% formic acid was used. Linear gradients from 7 to 38% B in 60 min were used for separation with a following increase to 80% B for 5 min and a re-equilibration to 5% B. Peptides were then sprayed into a tandem mass spectrometer, the Q Exactive plus (60). The resolution for MS1 spectra was 70 000 (mass range, 200–1200 m/z–1). MS1 spectra were acquired using 1E6 as an AGC target. MS/MS spectra of the top 10 most intense peaks were obtained by higher-energy collisional dissociation fragmentation. Resolution for MS/MS spectra was 35 000 at 200 m/z–1, AGC target was 5E5, max. injection time was 120 ms.

Bioinformatic analysis

RAW files generated by the QExactive tandem mass spectrometer were processed using MaxQuant, v.1.4.1.2 with default settings. Fixed modifications were carbamidomethylation on cysteins. Variable modification was Methionine oxidation. PSM, and site and protein false discovery rate (FDR) was 0.01. Minimal peptide length was 7. Match between run option and

label-free quantification option was enabled. Data was searched against a mouse uniprot database in fasta format from the Mus musculus, reference proteome downloaded from uniprot.org on 23rd of February 2014. MaxQuant output (proteingroups.txt file) was uploaded in Perseus, v. 1.6.7.0. Contaminants and reverse hits were removed. Determination of significant interactors was performed using a two-tailed t-test and FDR and s0 cutoff values indicated in the figure legends. Stoichiometry analysis was performed using intensity based absolute quantification (iBAQ) values.

Immunohistochemistry

Mouse kidney tissue was fixed in 10% (v/v) neutral-buffered formalin (Klinipath BV) in PBS for >24 h. Samples were dehydrated through alcohol (Klinipath BV), embedded in paraffin (39602004, Leica biosystems), and cut into 4- μ m sections. For immunohistochemistry of the kidney sections, deparaffinization and rehydration were performed, followed by permeabilization in PBS-Triton 0.3% (v/v) (Sigma). Sections were incubated overnight at 4°C with the primary antibodies sheep anti-NCC (1:400) (Sheep S965B, MRC PPU, Dundee), sheep anti-Tamm Horsfall (1:200) (MBS220487, Bio-Trend) and guinea pig anti-AQP2 (1:100) (kindly provided by dr. Peter Deen). Subsequently, sections were incubated for 2 h at room temperature with Alexa 594 conjugated secondary antibodies (1:300) (Thermo Fisher Scientific, Molecular Probes). For co-staining with RRAGD, sections were then blocked with 0.3% (v/v) H₂O₂ (Dentek) and Avidin/Biotin (SP-2001, Vector Labs) and subsequently incubated overnight at 4°C with the primary antibody rabbit anti-RRAGD (1:2,000) (NBP2-32106, Novus Biologicals). For detection of RRAGD, sections were incubated for 2 hours at room temperature with a swine anti rabbit Biotin SP-conjugated secondary antibody (1:2,000) (4050-08, Southern Biotech), followed by incubation with Streptavidin-HRP (1:100) and fluorescein tyramide (1:50) according to the manufacturers protocol (NEL741001KT, Perkin Elmer). Slides were mounted with Fluoromount-G with DAPI (0100-20, Southern Biotech).

DETAILED CLINICAL DESCRIPTION

Family 1

The boy was born at 38 weeks of gestation after normal pregnancy (normal amniotic fluid) by vaginal delivery. He was reportedly healthy during the first years of life receiving breast feeding for eight months followed by infant formula. There was no indication of vomiting, diarrhea, polyuria or dehydration. At 18 months of age he was admitted to a local hospital for a purple rash on his face and legs, and Henoch-Schonlein Purpura was diagnosed.

At 6 years of age, he presented to a tertiary hospital with a history of decreased oral intake, vomiting, abdominal pain and fatigue. He was found to have severe dilated cardiomyopathy and cardiac insufficiency that did not stabilize under intensive medical therapy and, 7 days after admission, necessitated the placement of a left ventricular assist device (25 mL Berlin heart). He was listed for high urgency cardiac transplant and received an orthotopic heart transplant 20 days later. Hypomagnesemia was first noted at admission. Renal evaluation after cardiac transplant confirmed renal magnesium wasting, renal ultrasound revealed bilateral medullary nephrocalcinosis. Analyses of serum and urine electrolytes indicated persisting hypomagnesemia due to renal magnesium wasting accompanied by hypercalciuria. All other electrolytes as well as acid base metabolism were within normal limits.

For the evaluation of dilated cardiomyopathy, genetic testing for copy number variations (CNVs) using a microarray as well as comprehensive testing for mutations using a cardiomyopathy gene panel were performed with negative results. In addition, a genetic testing of known hypomagnesemia genes (including *CLDN16*, *CLDN19*, *CNNM2*, *EGF*, *HNF1b*, and *TRPM6*) failed to detect pathogenic variants.

Family 2

A three-year-old girl (born 1985) presented in the clinic with tetanic convulsions. She had hypocalcemia (1.1 mmol/L) and hypomagnesemia (0.5 mmol/L). During disease manifestation elevated plasma renin activity (32 ng/ml/h) and aldosterone levels (1.57 ng/ml) were noted in the absence of clinical signs of salt and/or water loss (no polyuria/polydipsia) and blood pressure was normal. Despite a treatment with calcium and vitamin D supplements, serum calcium levels did not increase until magnesium supplementation was started. Thereafter, the tetanic convulsions stopped and serum calcium concentrations normalized while serum magnesium levels remained low. Further clinical and biochemical workup clearly demonstrated a renal magnesium loss as shown in two separate parenteral magnesium loading tests (Figure 1B). In addition, when serum calcium levels were normalized, repeated episodes of hypercalciuria (6 to 12 mg/kg/d) were noted, and she developed discrete medullary nephrocalcinosis. The girl was treated with magnesium supplementation, potassium citrate, and occasionally calcium. During follow-up, the compliance with therapy was poor and serum calcium levels fell below the normal range repeatedly. At the age of nine years, the girl withdrew therapy completely.

At 12 years of age, she developed heart failure and the diagnosis of dilated cardiomyopathy was established. In addition, severe hypomagnesemia (min. 0.19 mmol/L) was noted, while serum calcium levels and urinary calcium excretions were normal. An endomyocardial biopsy was performed and did not demonstrate any abnormal finding. The mitochondrial respiratory chain activity was normal. Supportive therapy was initiated with digoxin, furosemide, captopril and fludione. At 25 years of age, progressive heart failure necessitated external cardiac assistance. A few weeks later, she underwent successful heart transplantation. Histology of the explanted heart showed unspecific dilated cardiomyopathy.

Family analysis did not reveal further affected family members, blood and urinary magnesium levels of the parents were normal at several occasions. Renal ultrasound was normal in both

parents. Mild mitral regurgitation in the father and slight left ventricular hypertrophy in the mother were detected by echography.

Family 3

The girl was born at 35 weeks of gestation after a pregnancy complicated by polyhydramnios with a birth weight of 2580g. During the early neonatal period, she showed muscular hypotonia. An extensive metabolic work-up, brain MRI, electromyography, as well as genetic studies for Prader-Willi syndrome were performed with unremarkable findings. At 3 weeks of age, she presented with tachycardia (heart rate of 250 beats per minute). An echocardiogram revealed left ventricular dilation as well as a ventricular septal defect of 6mm with a gradient of 36mm. Heart failure treatment with digoxin and furosemide was initiated. At 9 months of age, the diagnosis of dilated cardiomyopathy was made (table 1). After a generalized cerebral seizure episode at 2 years of age, hypokalemia and hypomagnesemia were detected and furosemide treatment was stopped. The co-existence of polyuria and polydipsia along with an impaired renal urine concentrating ability suggested a renal tubular defect. Renal ultrasound revealed medullary nephrocalcinosis. Supplementation with oral potassium and magnesium was initiated. Her cardiac function intermediately stabilized under treatment with digoxin, lisinopril, and spironolactone. An endomyocardial biopsy did not reveal signs of mitochondrial disease. Unfortunately, her cardiac function deteriorated during further follow-up, she developed cardiac failure, and finally received a cardiac transplant at 15 years of age.

Serum magnesium levels have constantly remained low (0.4 to 0.5mmol/L) despite high dose oral magnesium supplementation. Furthermore, laboratory analyses during follow-up demonstrated hypokalemia despite continuous oral supplementation as well as mild metabolic alkalosis.

After extensive analyses of known genes for renal tubular disorders including renal salt and magnesium wasting yielded negative results, whole exome sequencing was performed and

analyzed together with the exomes of the individuals from families F1, F2, and F4 which finally identified the *RRAGD* gene as the single shared gene with pathogenic variants.

Family 4

The index case was born at 37 weeks of gestation with a weight of 2900g. There was marked polyhydramnios during pregnancy. Postnatally, polyuria was noted, but serum electrolytes remained normal. Moreover, there was no increased renin activity. At that time, there was no hypercalciuria nor nephrocalcinosis.

He presented in the clinic at 6 years of age with complaints of cramps and tetany. Laboratory findings revealed the presence of marked hypomagnesemia associated with hypokalemia. Serum calcium and sodium levels were within normal ranges.

Family analysis indicated that his father had hypokalemia, severe hypomagnesemia and nephrocalcinosis. He developed dynamic mitral valve dysfunction with severe left ventricular dysfunction. This evolved to dilated cardiomyopathy with biventricular dysfunction and he died at 41 years of age from cardiac insufficiency.

Family 5

After an uneventful pregnancy and birth, the girl showed feeding difficulties, emesis, and failure to thrive accompanied by paleness and sweating. An acute deterioration of her clinical status with tachycardia and tachypnea lead to admission to a local children`s hospital at 7 months of age. Under the suspicion of decompensated cardiac insufficiency, the girl was transferred to pediatric cardiology of a tertiary care hospital. Echocardiography on admission revealed a massively dilated left ventricle with a shortening fraction of <10%. Treatment for heart failure with furosemide, spironolactone, captopril, and digoxin was initiated which lead to a stabilization of cardiac function, however, the left ventricular shortening fraction remained low at 15-20%. An extensive work-up revealed no underlying metabolic abnormality or infectious cause; a cardiac

biopsy was performed without decisive findings. Hypomagnesemia (serum magnesium of 0.38mmol/L) was detected at 15 months of age during a hospitalization for an airway infection. Polyuria and polydipsia were first noted during the second year of life along with additional electrolyte abnormalities including hyponatremia and hypokalemia. Urine analyses revealed hypercalciuria, ultrasound examinations in the second year of life revealed nephrocalcinosis. The girl was closely followed by a pediatric cardiologist. Fortunately, her cardiac function remained stable to date (table 1) under heart failure medication with carvedilol, enalapril, spironolactone, and hydrochlorothiazide. Digoxin treatment was stopped at 5 years of age. Over the years, she required repeated hospitalizations for airway and urinary tract infections. Polyuria as well as electrolyte abnormalities with hypomagnesemia and hypokalemia persisted despite oral supplementation. Medullary nephrocalcinosis is mild (grade 1 to 2a according to Hoyer), her renal function is actually normal.

Genetic analysis using a custom multi-gene panel for 174 cardiovascular genes (Institute for the Genetics of Cardiac Disorders, Department of Cardiology, University Hospital Münster, Germany) did not reveal any pathogenic variants in known cardiomyopathy genes.

Family 6

The patient presented at the age of 14 years with chest pain and NYHA Class 1 dyspnea. At that time, the echocardiography showed hyperechogenicity of the interventricular septum, with a slightly reduced ejection fraction (EF; at ~50%). The cardiologic follow-up, including stress tests and magnetic resonance imaging (MRI) following adenosine infusion, did not reveal any signs of myocardial ischemia. Blood pressure (BP) levels remained chronically low (~90/60 mmHg). Laboratory analyses showed hypomagnesemia (0.42 mmol/L) and borderline hypokalemia (3.5 mmol/L). Kidney function was preserved, with no proteinuria. The patient was treated by perindopril and bisoprolol. At the age of 35 years, the patient developed a cardiogenic shock, with severely impaired left ventricular (LV) EF (at ~15%) and systolic BP levels < 80 mmHg, in the

context of pneumonia-induced sepsis. The implantation of a Boston defibrillator was necessarily performed. The patient progressively recovered to NYHA Class 2, and the latest echocardiography at the age of 36 years showed dilated cardiomyopathy (DCM) with LV EF of 45% under sacubitril/valsartan, spironolactone, bumetanide and bisoprolol. Laboratory analyses showed normal serum potassium levels, but low serum magnesium levels (0.62 mmol/L) despite oral supplementation. The father of the patient had died at the age of 33 years from myocardial infarction in a context of untreated hypercholesterolemia and poorly controlled type 2 *diabetes mellitus*. On the basis of the hetero-anamnesis of the spouse, there was no indication of DCM since the cardiac check-up performed few months before the patient died was considered as normal. The mother of the patient was asymptomatic. Her kidney function was preserved. The echocardiography showed no dilation of the cardiac cavities, with a 58% EF. The patient's grandfather and paternal uncle both died of sudden death at the age of 26 and 19 years, respectively. The autopsy of the uncle disclosed congestive DCM, with multiple intra-cardiac thromboses in a putative context of viral myocarditis. No precise clinical or biological or genetic information could be obtained about these 2 cases.

Family 7

The index patient was born at 38 weeks of gestation by caesarian section with a birth weight of 4250g. During pregnancy, the mother had developed gestational diabetes. The family history was remarkable for an older sister who had died in infancy during an acute febrile episode.

In infancy, she presented with recurrent episodes of vomiting, feeding problems, and failure to thrive. Lactose intolerance was diagnosed and she received lactose-free formula nutrition. At 2 years of age, she was admitted to a local hospital for acute gastroenteritis. Abdominal ultrasound revealed bilateral medullary nephrocalcinosis. Serum electrolytes were remarkable for an increased serum calcium of 2.9mmol/L, serum magnesium levels were not determined. Three months later, she was referred to a pediatric nephrology department for a diagnostic work-up of

her nephrocalcinosis. At that time, hypomagnesemia (0.62 mmol/L) was detected, while all other electrolytes were within normal limits (table 1). An evaluation of mineral metabolism revealed an increased intact PTH of 90.8 pg/mL, urine analyses indicated combined renal calcium and magnesium wasting. A supplementation with oral magnesium citrate was initiated. Under the suspicion of familial hypomagnesemia with hypercalciuria and nephrocalcinosis (FHHNC; MIM #248190), genetic testing was performed which excluded mutations in *CLDN16* and *CLDN19* genes. During follow-up, feeding improved and the patient grew between the 10th and 25th percentile for height and weight. Nephrocalcinosis as well as hypomagnesemia and renal calcium and magnesium wasting persisted. Due to the unknown etiology of her renal phenotype, the patient was subjected to whole exome sequencing. The analysis of her single exome at that time did neither reveal pathogenic variants in known genes for hypomagnesemic disorders nor, after sequential filtering, any promising coding gene variants in homozygous or compound-heterozygous state (under the assumption of recessive inheritance).

After discovery of *RRAGD* variants in families F1 to F3, the re-analysis of her exome revealed the p.Pro119Leu variant in *RRAGD* in heterozygous state. The molecular diagnosis prompted a cardiac evaluation which revealed a dilated left ventricle with impaired pump function (FS 18%) and mitral regurge grade 1 to 2. Fortunately, a heart failure therapy with lisinopril and spironolactone resulted in a stabilization of her cardiac function and improvement of her clinical status. Since then, she is closely followed by pediatric cardiology and nephrology departments. Hypokalemia detected during a recent follow-up visit (at 5 years of age) resulted in an oral potassium supplementation in addition to magnesium. Nephrocalcinosis is stable, her renal function normal.

A re-evaluation of the autopsy report of her older sister revealed dilative cardiomyopathy with suspected acute cardiac failure in the context of a pneumonia. Unfortunately, DNA from her sister was not available. However, an analysis of the parents` DNA was initiated under the assumption of dominant inheritance. Conventional Sanger sequencing demonstrated an uncertain pathologic

peak at the position of the patient's mutation in the *RRAGD* gene in her mother. Next-generation sequencing (see above, Supplemental Methods) revealed the *RRAGD*-c.356C>T variant in 17% of analyzed reads indicating maternal mosaicism for the p.Pro119Leu mutant. An echocardiography of the mother was normal with an ejection fraction (EF) of 55%. She is treated with an ACE inhibitor for familial essential hypertension.

Family 8

The patient originates from a Turkish family with parental consanguinity. Two apparently healthy sisters as well as the parents do not display electrolyte abnormalities or signs of renal salt or water loss. The patient was born at term with a birth weight of 3800g. The infancy period was characterized by episodes of vomiting and fever, however, no detailed laboratory analyses were performed in local hospitals. He clinically presented at 6 years of age with a cerebral seizure. At that time, laboratory analyses revealed hypomagnesemia, hypokalemia, and hypocalcemia. In addition, metabolic alkalosis was present. Renal ultrasound was remarkable for medullary nephrocalcinosis. Potassium as well as magnesium supplementation was initiated. Genetic studies by conventional Sanger sequencing failed to detect pathogenic variants in genes for renal salt wasting (Bartter syndrome) as well as in *CLDN16* or *CLDN19* (FHHNC). Follow-up examinations demonstrated persisting hypokalemia and hypomagnesemia despite oral supplementation. Urinary analyses indicated varying calcium excretions, serum intact PTH levels were mostly within the normal range with single elevated values.

The patient is now 21 years old. His weight is 84 kg and his height 162cm (BMI of 32 kg/m²). He displays stable serum potassium levels, but persisting hypomagnesemia under oral supplementation (table 1). He actually is a college student.

After excluding mutations in known genes for renal salt wasting and hypomagnesemia, he was subjected to whole exome sequencing (single exome). No promising variants were detected under the assumption of autosomal-recessive inheritance because of parental consanguinity. His

exome was re-analyzed after discovery of *RRAGD* mutations in families 1 to 5. After discovery of the genetic defect in *RRAGD*, he was clinically re-evaluated including a cardiac work-up. Echocardiography demonstrated an unremarkable cardiac function and no signs of cardiomyopathy. A 24-h blood pressure monitoring (ABPM) demonstrated arterial normotension.

Family 9

The index patient of Family 9 (#III.3 in Supplementary Figure 1. Panel A) initially presented with muscular cramps, tetany and excessive muscular fatigability at the age of 20 years. No polyuria or polydipsia was reported. In addition, tooth erosions were noted. Blood pressure (BP) levels were in the lower range, i.e. 90/60 mmHg. Laboratory analyses showed hypomagnesemia (0.46 mmol/L), hypokalemia (3.5 mmol/L) and metabolic alkalosis ($[\text{HCO}_3^-]$, 35 mmol/L) (Supplementary Table 1). Kidney function was preserved, with no proteinuria. No kidney stones or nephrocalcinosis was documented. The cardiologic follow-up (until the age of 45 years) was unremarkable, with homogenous LV contractility and 78 % ejection fraction. His father (#II.9, symptomatic at the age of 20 years), as well as his paternal aunt (#II.6, symptomatic at the age of 24 years) and uncle (#II.5, symptomatic at the age of 20 years), showed a similar phenotype of hypomagnesemia-associated tetany, with no evidence for cardiac abnormalities or renal calcium deposits (Supplementary Table 1). Of note, their BP levels were also in the lower range (~90/60 mmHg).

The cousin (#III.1) of the index case presented with muscular cramps at the age of 10 years in the context of polyuria. Water restriction test showed no response to arginine-vasopressin administration. At the age of 21 years, the patient presented with a first episode of a renal colic. Follow-up (until the age of 29 years) showed recurrent formation of calcium-containing kidney stones, with no nephrocalcinosis *stricto sensu*. BP levels were in the lower range, i.e. 90/60 mmHg. Laboratory analyses showed hypomagnesemia (0.42 mmol/L), hypokalemia (3.4 mmol/L), and metabolic alkalosis ($[\text{HCO}_3^-]$, 28 mmol/L) (Supplementary Table 1). Kidney function

was preserved, with no proteinuria. The patient was asymptomatic as far as the heart is concerned. No echocardiography has been performed thus far.

The index patient (#III.3) had 4 children (IV.1-4) with 3 different wives, of whom 2 presented with hypomagnesemia. The little girl IV.2 was born in a context of polyhydramnios that required multiple drainages. Still, she did not develop polyuria or enuresis in childhood. At the age of 16 years, she presented with tetany. BP levels were low (<90/60 mmHg), with recurrent episodes of symptomatic BP drops. Laboratory analyses showed hypomagnesemia (0.56 mmol/L), hypokalemia (3.4 mmol/L) and metabolic alkalosis ($[\text{HCO}_3^-]$, 28 mmol/L) (Supplementary Table 1). Kidney function was preserved, with no proteinuria. No kidney stones or nephrocalcinosis have been documented. The patient was asymptomatic from the cardiac point of view. No echocardiography has been performed thus far. Finally, the little girl IV.4 presented with asymptomatic hypomagnesemia (0.62 mmol/L) discovered in the context of the present study at the age of 4 years. Note that serum magnesium levels were normal at the age of 2 years, similarly to patient III.6 who showed normomagnesemia at the age of three months but developed symptomatic hypomagnesemia with cramps and tetany at the age of 12 years. All members of Family 9 who were tested negative for the c.289A>C (p.Thr97Pro) *RRAGD* mutation, including II.4, II.8, II.10, III.2, IV.1 and IV.3, did not show any abnormalities in kidney or heart functions. There was no case of sudden death in Family 9.

DETAILED STRUCTURE DISCUSSION

All variants are found in the N-terminal G-domain and affect sequence motifs involved in nucleotide binding (Figure 1E). These motifs are highly conserved within small G-proteins and are proven to be important for high affinity nucleotide binding.⁷ Ser76 is part of the G1 motif, also known as P-loop, Thr97 constitutes the G2 motif and Pro119 resides in the G3 motif (Figure 1E-G). These motifs are involved in the interaction with the phosphate moiety of the nucleotide. Ile221 resides in a sequence stretch corresponding to the G5 motif. Though the consensus of G5 is not fully conserved in RagD, the region is functionally conserved as it interacts with the base of the nucleotide (Figure 1G). The variants are expected to display low nucleotide affinity and fast nucleotide exchange. This may interfere with RagD mediated signaling in different manners. First, nucleotide free G-proteins display high affinity for GEFs. Therefore, variants with low nucleotide affinity can act as dominant negative by trapping GEFs. However, GEFs for RagD are unknown and this effect requires, that the mutation is not interfering with the interaction between GEF and G-protein per se. Second, nucleotide free G-proteins are typically unstable and thus the RagD variants may be degraded. Third, due to the enhanced nucleotide exchange rate a higher fraction of the RagD variants may be GTP loaded than of wild type RagD. As consequence RagD•GTP dependent signaling may be enhanced. However, this effect requires, that the interaction between RagD-GTP and effector proteins is not perturbed. The mutations result in amino acid residues that are sterically more demanding and at least in some cases are incompatible with the fold observed in a crystal structure of human RagD (pdb entry 2q3f), where switch I is folded over the nucleotide. Such a closed conformation is typically found in GTP- or GDP-bound small G-proteins.⁷ During nucleotide exchange switch I adopts an open conformation and a close and an open conformation of switch I were observed in the yeast homolog of RagD.⁸⁻¹⁰ The open conformation would be compatible with the steric demand of the variants, but likely not with effector interaction.

REFERENCES

1. Altmuller J, Motameny S, Becker C, et al. A systematic comparison of two new releases of exome sequencing products: the aim of use determines the choice of product. *Biol Chem* 2016;397:791-801.
2. Hart SN, Duffy P, Quest DJ, Hossain A, Meiners MA, Kocher JP. VCF-Miner: GUI-based application for mining variants and annotations stored in VCF files. *Brief Bioinform* 2016;17:346-51.
3. Cottingham RW, Jr., Idury RM, Schaffer AA. Faster sequential genetic linkage computations. *Am J Hum Genet* 1993;53:252-63.
4. Lathrop GM, Lalouel JM, Julier C, Ott J. Strategies for multilocus linkage analysis in humans. *Proc Natl Acad Sci U S A* 1984;81:3443-6.
5. Rinschen MM, Bharill P, Wu X, et al. The ubiquitin ligase Ubr4 controls stability of podocin/MEC-2 supercomplexes. *Hum Mol Genet* 2016;25:1328-44.
6. Rappsilber J, Ishihama Y, Mann M. Stop and go extraction tips for matrix-assisted laser desorption/ionization, nanoelectrospray, and LC/MS sample pretreatment in proteomics. *Anal Chem* 2003;75:663-70.
7. Vetter IR, Wittinghofer A. The guanine nucleotide-binding switch in three dimensions. *Science* 2001;294:1299-304.
8. Bos JL, Rehmann H, Wittinghofer A. GEFs and GAPs: critical elements in the control of small G proteins. *Cell* 2007;129:865-77.
9. Gong R, Li L, Liu Y, et al. Crystal structure of the Gtr1p-Gtr2p complex reveals new insights into the amino acid-induced TORC1 activation. *Genes Dev* 2011;25:1668-73.
10. Jeong JH, Lee KH, Kim YM, Kim DH, Oh BH, Kim YG. Crystal structure of the Gtr1p(GTP)-Gtr2p(GDP) protein complex reveals large structural rearrangements triggered by GTP-to-GDP conversion. *J Biol Chem* 2012;287:29648-53.

SUPPLEMENTARY TABLE 1

Family 9	II.4	II.5	II.6	III.1	II.9	III.3	III.6	IV.1	IV.2	IV.3	IV.4
General parameters											
Gender	F	M	F	M	M	M	F	M	F	F	F
Age at manifestation (y)	-	20	24	10	20	20	12	-	10	-	
Hypomagnesemia-related symptoms	No	tetany	tetany	muscular cramps	tetany	muscular cramps, tetany	muscular cramps, tetany	No	tetany	No	No
Dilated Cardiomyopathy (DCM)	No	No	No	No	No	No	No	No	No	No	No
Hypercalciuria/ Nephrocalcinosis			No	Yes	No	No	No	?	No	No	No
Polyuria		No	No	Yes	No	No		No	No	No	No
Metabolic alkalosis			Yes	Yes	?	Yes	Yes	?	No	No	?
Initial laboratory findings:											
S-Na (mmol/L)		139	140	139	140	140	140	138	138	142	138
S-K (mmol/L)		3.2	3.6	3.1	3.2	3.5	2.7	5	3.4	4.2	4.0
S-Cl (mmol/L)	104	99	98	99	91	95	98	103	101	106	101
S-Ca (mmol/L)		2.3	2.5	2.2	2.4	2.4	2.2	2.5	2.3	2.4	2.6
S-Mg (mmol/L)		0.53	0.41	0.34	0.32	0.54	0.45		0.59	0.84	0.76
S-PO ₄ (mmol/L)		0.82	0.97			0.87	1.20		1.12	1.7	
S-creatinine (mg/dL)	0.64	0.52	0.45	0.40	0.69	0.74	0.60	0.40	0.35	0.50	0.30
S-HCO ₃ (mmol/L)							29.6				
iPTH (pg/mL)						21	16		17		
FE-Na (%)						0.4	0.3		0.5		
FE-K (%)						7.5	5.7		5.4		
Ca/Crea-ratio (mol/mol)				calciuria 5mg/kg/ 24h	calciuria 300mg/24h	0.25			0.06		
FE-Mg (%)											

Follow-up											
Age at last follow-up (yr)	56	50	49	27	61	40	18	16	16	13.5	4
Heart Transplant (Age)	No	No	No	No	No	No	No	No	No	No	No
ejection fraction (EF)	>65%	60%	71%		65%	78%					
left ventricular end-diastolic diameter (LVEDD)	no dilation		no dilation		no dilation	no dilation					
Most recent laboratory findings:											
S-Na (mmol/L)	142	140	141	140	140	140	142	142	139	141	138
S-K (mmol/L)	3.92	3.4	3.5	3.4	3.1	3.53	3.2	4.3	3.45	4.2	3.8
S-Cl (mmol/L)		95	98	99	92	97			100	108	99
S-Ca (mmol/L)	2.39	2.5	2.5	2.3	2.2	2.3	2.4	2.6	2.43	2.5	2.6
S-Mg (mmol/L)	0.84	0.53	0.34	0.42	0.36	0.46	0.54	0.87	0.56	0.94	0.62
S-creatinine (mg/dL)	0.6	0.47	0.5	0.7	0.9	0.7	0.51	0.8	0.5	0.5	0.3
S-HCO ₃ (mmol/L)		23.4	34.7	27.9		35	30.4		27		28
iPTH (pg/mL)			15.6	25.4	10.2	18	11.6		26		13.3
FE-Na (%)	1.15		0.72	0.48	0.66	0.77	0.41		0.39		
FE-K (%)	15.6		10.84	12.95	13.63	12.1	7.37		7.4		
Ca/Crea-ratio (mol/mol)											
FE-Mg (%)	1.6		7.44	4.52	7.02	5.9	3.75		2.8		
Therapy											
Magnesium therapy	No	Yes	Yes	Yes	No	Yes	Yes	No	Yes	No	No
Potassium therapy	No	Yes	Yes	Yes	No	No	No	No	No	No	No
Heart Failure Medication/ Immunosuppressants	No	No	No	No	No	No	No	No	No	No	No
Genetic Findings (RRAGD mutations)											
Nucleotide level	wt	c.289G>A	c.289G>A	c.289G>A	c.289G>A	c.289G>A	c.289G>A	wt	c.289G>A	wt	c.289G>A
Protein level	wt	p.Thr97Pro	p.Thr97Pro	p.Thr97Pro	p.Thr97Pro	p.Thr97Pro	p.Thr97Pro	wt	p.Thr97Pro	wt	p.Thr97Pro
Inheritance		dominant	dominant	dominant	dominant	dominant	dominant		dominant		dominant

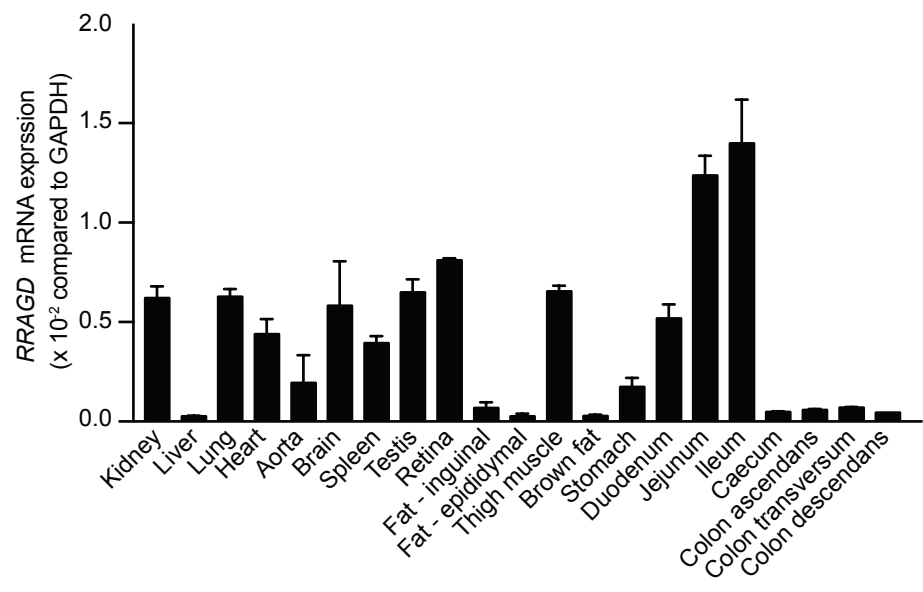
Supplementary table 2: Interactome RagD-p.Ser75Leu vs. RagD-wt

Protein name	Gene name	Difference
Mitogen-activated protein kinase kinase kinase 19	Map3k19	5.8385
Ragulator complex protein LAMTOR3	Lamtor3	3.3500
Flotillin-2	Flot2	3.1498
Regulatory-associated protein of mTOR	Rptor	3.0583
Retinoic acid-induced protein 3	Gprc5a	2.8338
V-type proton ATPase subunit E 1	Atp6v1e1	2.7697
Ragulator complex protein LAMTOR2	Lamtor2	2.6929
Type 1 phosphatidylinositol 4,5-bisphosphate 4-phosphatase	Tmem55b	2.5940
Ragulator complex protein LAMTOR5	Lamtor5	2.5223
Serum albumin	Alb	2.4787
V-type proton ATPase subunit B, brain isoform	Atp6v1b2	2.4520
Claudin-3	Cldn3	2.3405
V-type proton ATPase catalytic subunit A	Atp6v1a	2.3375
V-type proton ATPase subunit d 1	Atp6v0d1	2.3149
Eukaryotic initiation factor 4A-I;Eukaryotic initiation factor 4AII; Eukaryotic initiation factor 4A-II, N-terminally processed	Eif4a1;Eif4a2	2.3109
V-type proton ATPase subunit a	Tcirg1	2.3028
Major facilitator superfamily domain-containing protein 1	Mfsd1	2.1601
Flotillin-1	Flot1	2.0361
Type 2 phosphatidylinositol 4,5-bisphosphate 4-phosphatase	Tmem55a	2.0265
V-type proton ATPase subunit G 1	tp6v1g1	1.9777
Phosphate carrier protein, mitochondrial	Slc25a3	1.8957
Protein FAM32A	Fam32a	1.8091
V-type proton ATPase subunit H	Atp6v1h	1.7714
Lamin-B receptor	Lbr	1.4967
BAG family molecular chaperone regulator 2	Bag2	1.4151
tRNA-splicing ligase RtcB homolog	Rtcb	-1.6719
Bromodomain-containing protein 1	Brd1	-1.7355
Cullin-4B	Cul4b	-1.7555
Myosin phosphatase Rho-interacting protein	Mprip	-1.8521
Periodic tryptophan protein 2 homolog	Pwp2	-1.9179
U3 small nucleolar RNA-associated protein 6 homolog	Utp6	-2.4039
Probable ATP-dependent RNA helicase DDX10	Ddx10	-2.8054

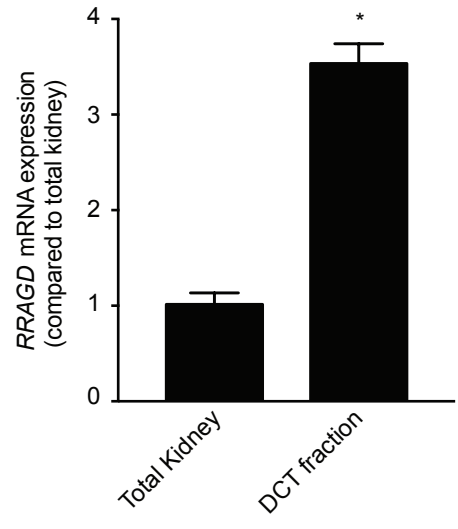
Supplementary figure 1

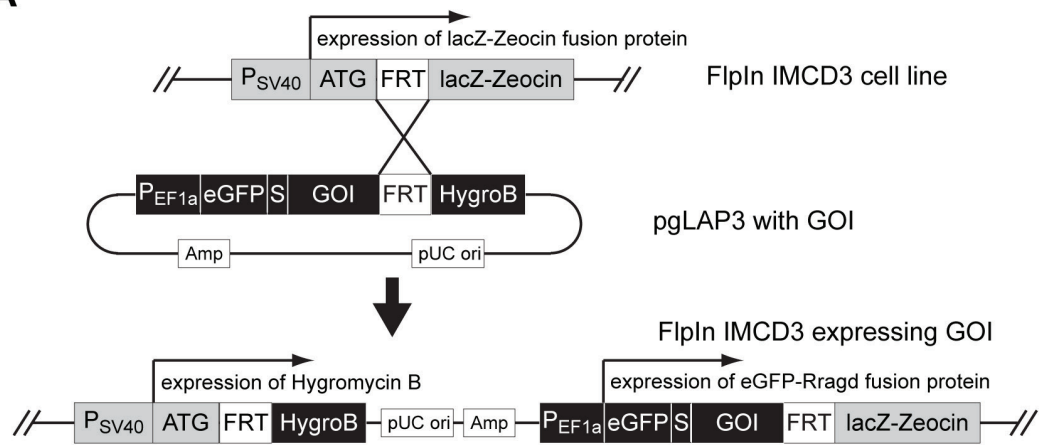
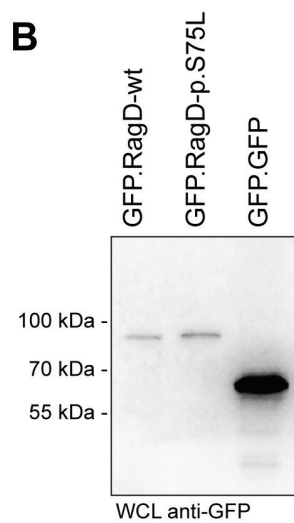
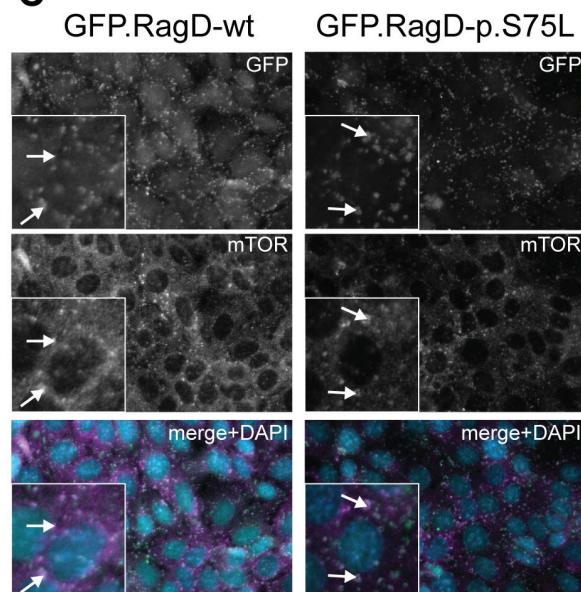
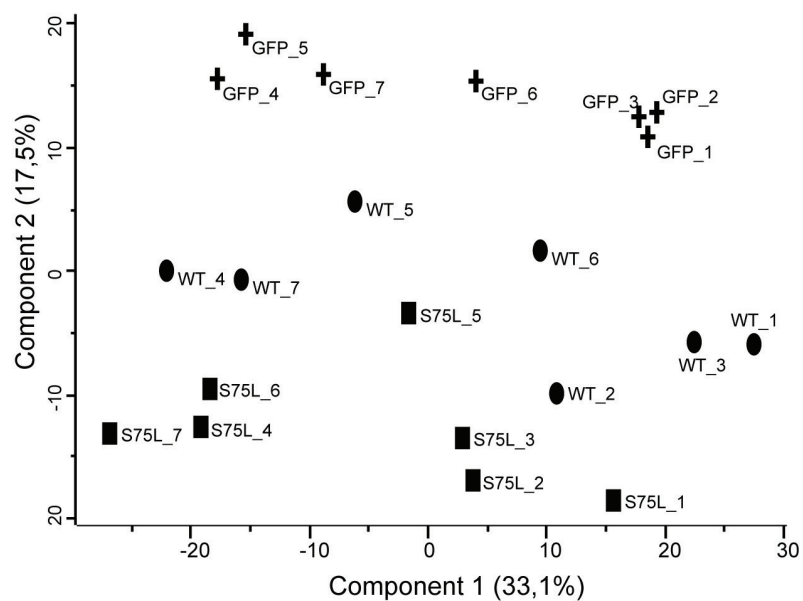
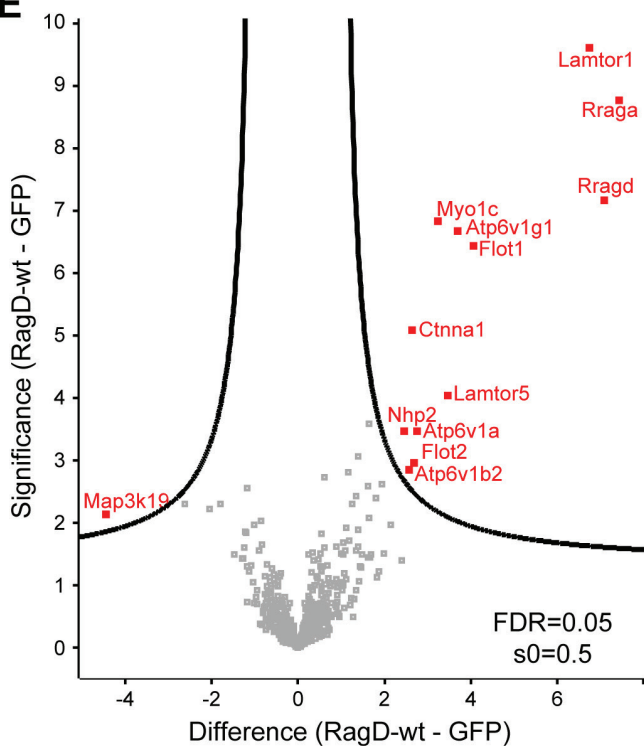
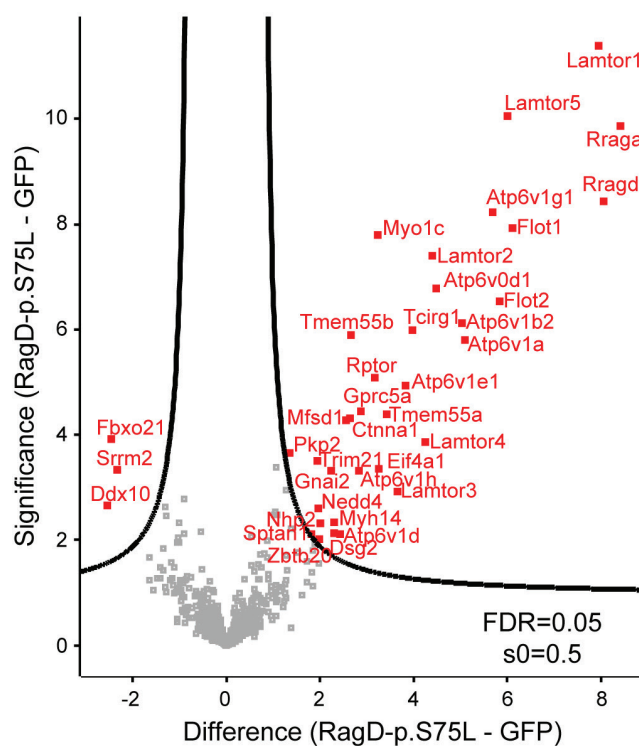
S. Cerevisiae	-----M	1
C. Elegans	-----MESDPD-----EDFDDYRYGIDE-----	18
D. Melanogaster	-----MSYDDDDYPADTFPKDFGYRAYNQDGLLEPN	32
D. Rerio	-----MTSARKNNEVDG---ENEALSFDDYDDDD-DFDAFTD--GDGDCSCDGGVGLGFS	48
X. Tropicalis	-MSLPGKSH-ERQEEEEGDDEDDIMGVSDYG---DGDSFMD--GERGSEGDDVEVLDFT	52
M. Musculus	MSQVLGKPPQGEDGGE-DEEDELVGLAGYE---DGPSSD--AELDSGPEEGVLDIFS	53
H. Sapiens	MSQVLGKPPQVEDDAEEEEEEDELVGLADYG---DGPSSD--ADPDSGTTEEGVLDIFS	54
	<i>G1-Box</i> <i>G2-Box</i>	
S. Cerevisiae	SLEATDSKAMVLLMGVRRCGKSSICKVVFHNMQLDLYLESISNPSLEHF--STLIDLA	59
C. Elegans	EDDYPDSRPTVILMGHKRSGKTSIRKVVVFQKMSPNETMFVESTARITRDTI-CSSFINF	77
D. Melanogaster	ATGSSETKPRILLMGMRRSGKSSIQKVVVFHKMSPNETLFLESTKIVKDDINNSFFVQFQ	92
D. Rerio	DPFSEVKPRILLMGLRRSGKSSIQKVVVFHKMSPNETLFLESTNKICREDVSNSSFFVSFQ	108
X. Tropicalis	DPFSTEKPRILLMGLRRSGKSSIQKVVVFHKMSPNETLFLESTNKICREDVSNSSFFVNFQ	112
M. Musculus	DPFSTEKPRILLMGLRRSGKSSIQKVVVFHKMSPNETLFLESTNRICREDVSNSSFFVNFQ	113
H. Sapiens	DPFSTEKPRILLMGLRRSGKSSIQKVVVFHKMSPNETLFLESTNKICREDVSNSSFFVNFQ	114
	<i>G3-Box</i>	
S. Cerevisiae	VMELFGQLNYFEPYSYDSEFLKSVGALVYVIDSQDEYINAITNLAMIIEYAYKVNPSINI	119
C. Elegans	TIEFPGQMCPPDSDLPVGVFQKCEALLFIIDAQAELEPIATLVEYFCRAYKINQNIKF	137
D. Melanogaster	IWDFPQIDDFEPTFDSDMIFGGCGALVFVIDAKDDYNEALTKFKNTVLQAYKVNKRIKF	152
D. Rerio	IWDFPQIDDFDPTFDYEMIFRGTGALIFVIDSQDDYVEALSRLHLTVTRAYKVNPDINF	168
X. Tropicalis	IWDFPQIDDFDPTFDYEMIFRGTGALIFVIDSQDDYMEALARLHLTVTSAYKVNPDINF	172
M. Musculus	IWDFPQIDDFDPTFDYEMIFRGTGALIFVIDSQDDYMEALARLHLTVTRAYKVNPDINF	173
H. Sapiens	IWDFPQIDDFDPTFDYEMIFRGTGALIFVIDSQDDYMEALARLHLTVTRAYKVNPDINF	174
	<i>G4-Box</i> <i>G5-Box</i>	
S. Cerevisiae	EVLIHKVDGLSEDFKVAQRDIMQRTGEELLEGLDGVQVSFYLTSTIFDHSIYEAFSRIV	179
C. Elegans	EVFVHKADGLTEEARVETKFNIIHQVKETIKDQIDVDLQVTYHLTSTIYDHSIFEAFSKVV	197
D. Melanogaster	EVFIHKVDGSISSDKMESQRDIHQRSSDDLNEAGLDQIHL SFHLSIYDHSIFEAFSKVV	212
D. Rerio	EVFIHKVDGLSDDHKIETQRDIHQRANDDLADAGLERIHL SFYLSIYDHSIFEAFSKVV	228
X. Tropicalis	EVFIHKVDGLSDDHKIETQRDIHQRANDDLVADGLEKIHLSFYLSIYDHSIFEAFSKVV	232
M. Musculus	EVFIHKVDGLSDDHKIETQRDIHQRANDDLADAGLEKIHLSFYLSIYDHSIFEAFSKVV	233
H. Sapiens	EVFIHKVDGLSDDHKIETQRDIHQRANDDLADAGLEKIHLSFYLSIYDHSIFEAFSKVV	234
	<i>G6-Box</i>	
S. Cerevisiae	QKLIPELSFLNMLDNLIQHSKIEKAFLFDVNSKIYVSTDSNPVDIQMYEVCSEFIDVTI	239
C. Elegans	QNLVKQLPTLERLLDVFNNSSKVTKSFLFDILSKIIYIATDSEPVEMSIYELCCDMIDVTL	257
D. Melanogaster	QKLIPQLPTLENLLNIFISNSGIEKAFLFDVNSKIYIATDSSPVDMQTYELCCDMIDVVI	272
D. Rerio	QKLIPQLPTLENLLNIFISNSGIEKAFLFDVNSKIYIATDSSPVDMQTYELCCDMIDVVI	288
X. Tropicalis	QKLIPQLPTLENLLNIFISNSGIEKVFVLDVNSKIYIATDSSPVDMQTYELCCDMIDVVI	292
M. Musculus	QKLIPQLPTLENLLNIFISNSGIEKAFLFDVNSKIYIATDSTPVDMQTYELCCDMIDVVI	293
H. Sapiens	QKLIPQLPTLENLLNIFISNSGIEKAFLFDVNSKIYIATDSTPVDMQTYELCCDMIDVVI	294
	<i>G7-Box</i>	
S. Cerevisiae	DLFDLYKAPVLRNSQKSSDKDNVINPRNELQNVSQLANGVIIYLRQMIRGLALVAIRPN	299
C. Elegans	DLSSYGVAAEN--G-----SNYDERSSSVIRLKSEQVMFLRQVNKHLALVFIMKED	306
D. Melanogaster	DLSSYSSSE---E-----TAFDSGSSSLIKLNNTTILYLREVNKFLALVCILREE	319
D. Rerio	DISCIYGLSGDEGG-----TPYDKESMAIHLNNTTVMYLKEVTKFLALVCFREE	339
X. Tropicalis	DISCIYGLE--GAG-----TPYDKESLAIKLNNTTIVLKEVTKFLALVCFVREE	341
M. Musculus	DISCIYGLKEDGAG-----APYDKDSTAIKLNNTTIVLKEVTKFLALVCFVREE	344
H. Sapiens	DISCIYGLKEDGAG-----TPYDKESTAIKLNNTTIVLKEVTKFLALVCFVREE	345
	<i>G8-Box</i>	
S. Cerevisiae	GTMESCLTVADYNIDIFKKGLEDIWANARASQAKNSIEDDV-----	341
C. Elegans	GNEKA---GFIDHNFVGFKAGIEQVFKVKNRGNF-----	338
D. Melanogaster	NFNRQ---GVIDYNFICFRDAISEVFEFLRLKRQKLENNDDDDDLVDEQTLIRHGHGADG	376
D. Rerio	SFEKK---GLIDYNFHCFKKAIEEVFVRLKVRQSRKLLSQRWRSR----QTPVN-----	387
X. Tropicalis	SFERK---GLIDYNFHCFRKAIQEVFEVRVKVLRSRKHQSQTKKSRSR----RATPN-----	389
M. Musculus	SFERK---GLIDYNFHCFRKAIHEVFEVRMVMKSRKAQSRLPKKT----GATPN-----	392
H. Sapiens	SFERK---GLIDYNFHCFRKAIHEVFEVRMVMKSRKVVQNRLLQKKK----RATPN-----	393
	<i>G9-Box</i>	
S. Cerevisiae	-----	341
C. Elegans	-----	338
D. Melanogaster	GISRAQPIN	385
D. Rerio	GTQV-LPH-	394
X. Tropicalis	GTPG-VPL-	396
M. Musculus	GTPR-VLL-	399
H. Sapiens	GTPR-VLL-	400

A



B



A**B****C****D****E****F**

SUPPLEMENTARY FIGURES

Supplementary Figure 1. Alignment of RagD shows mutations affect conserved residues

Clustal Omega alignment of Human RagD (Homo Sapiens Q9NQL2), Mouse RagD (Mus Musculus Q7TT45), Frog RagD (Xenopus Tropicalis Q0VFL0), Zebrafish RagD (Danio Rerio F1QIB5), Fruitfly RagC-D (Drosophila Melanogaster Q7K519), Worm RagC (Caenorabditis Elegans G5EGB3) and Yeast GTP-binding protein GTR2 (Saccharomyces Cerevisiae P53290). GTP-binding domains (G-boxes 1-5) are indicated in light blue. The residues affected by mutations are all within GTP-binding domains and are highlighted by a blue bar.

Supplementary Figure 2. *RRAGD* (RagD) is expressed in the heart and in the distal renal tubule

(A) mRNA expression levels of *Rragd* in a panel of mouse tissues measured by RT-qPCR and normalized for *Gapdh* expression. Data represent the mean of 3 individual experiments \pm SEM.

(B) The mRNA expression levels of *Rragd* were measured by RT-qPCR and normalized for *Gapdh* expression. DCT segments were selected by COPAS sorting and non-selected tubules served as control. Data represent the mean of 3 individual experiments \pm SEM and are expressed as fold differences compared to the non-selected tubules.

Supplementary Figure 3. Analysis of the RagD interactome

(A) Cloning strategy for the generation of FlpIn-IMCD cell lines with stable single-copy genomic integration of either GFP-RagD-WT, GFP-RagD-p.Ser75Leu or GFP-GFP. (B). Western blot analysis showing expression of GFP-RagD-WT or GFP-RagD-p.Ser75Leu transgenes in equal levels. (C) Immunofluorescence stainings show localization of GFP-RagD-WT or GFP-p.Ser75Leu (green) in vesicle-like structures, and co-localization with mTOR (magenta). (D) Principal component analysis demonstrates clear separation between GFP-GFP samples and

GFP-RagD samples. **(E-F)** Analysis of GFP-RagD-WT or GFP-RagD-p.Ser75Leu interactome (n=7). GFP-RagD-WT or GFP-RagD-p.Ser75Leu were immunoprecipitated and interactome was analyzed by label-free quantitative proteomics. In the volcano plots the significance (p-value) between GFP-RagD-WT or GFP-RagD-p.Ser75Leu vs GFP-GFP (-log₁₀ scale) is plotted against the difference (fold change) between GFP-RagD-WT or GFP-RagD-p.S75L vs. GFP-GFP (log₂ scale). Dots beyond the curved line represent proteins with significantly increased abundance (FDR 0.05, s₀=0.5).